



Aberystwyth University

Modelling Sex-Specific Crossover Patterning in Arabidopsis

Lloyd, Andrew; Jenczewski, Eric

Published in:
Genetics

DOI:
[10.1534/genetics.118.301838](https://doi.org/10.1534/genetics.118.301838)

Publication date:
2019

Citation for published version (APA):

Lloyd, A., & Jenczewski, E. (2019). Modelling Sex-Specific Crossover Patterning in Arabidopsis. *Genetics*, 211(3), 847-859. <https://doi.org/10.1534/genetics.118.301838>

General rights

Copyright and moral rights for the publications made accessible in the Aberystwyth Research Portal (the Institutional Repository) are retained by the authors and/or other copyright owners and it is a condition of accessing publications that users recognise and abide by the legal requirements associated with these rights.

- Users may download and print one copy of any publication from the Aberystwyth Research Portal for the purpose of private study or research.
- You may not further distribute the material or use it for any profit-making activity or commercial gain
- You may freely distribute the URL identifying the publication in the Aberystwyth Research Portal

Take down policy

If you believe that this document breaches copyright please contact us providing details, and we will remove access to the work immediately and investigate your claim.

tel: +44 1970 62 2400
email: is@aber.ac.uk

1 **Modelling sex-specific crossover patterning in Arabidopsis**

2

3 Andrew Lloyd^{*,†} and Eric Jenczewski[†]

4

5 ^{*}Institute of Biological, Environmental and Rural Sciences, Aberystwyth University,

6 Aberystwyth, SY23 3EB, UK

7 [†] Institut Jean-Pierre Bourgin, INRA, AgroParisTech, CNRS, Université Paris-Saclay, 78000,

8 Versailles, France.

9 **Short Title: Modelling crossovers in Arabidopsis**

10

11 **Keywords:** recombination, crossovers, interference, beam-film, sex-specific

12

13 **Corresponding author:** Andrew Lloyd

14

15 *Address:* Institute of Biological, Environmental and Rural Sciences, Plas Gogerddan,

16 Aberystwyth University, Aberystwyth, SY23 3EB, UK

17

18 *Phone:* +44 (0) 1970823229

19

20 *Email:* anl50@aber.ac.uk

ABSTRACT

21
22
23
24
25
26
27
28
29
30
31
32
33
34
35
36
37

Interference is a major force governing the patterning of meiotic crossovers. A leading model describing how interference influences crossover-patterning is the beam film model, a mechanical model based on the accumulation and redistribution of crossover-promoting stress along the chromosome axis. We use the beam-film model in conjunction with a large Arabidopsis reciprocal back-cross data set to gain mechanistic insights into the differences between male and female meiosis and crossover patterning. Beam-film modelling suggests that the underlying mechanics of crossover patterning and interference are identical in the two sexes, with the large difference in recombination rates and distributions able to be entirely explained by the shorter chromosome axes in females. The modelling supports previous indications that fewer crossovers occur via the class II pathway in female meiosis and that this could be explained by reduced DNA double strand breaks in female meiosis, paralleling the observed reduction in synaptonemal complex length between the two sexes. We also demonstrate that changes in the strength of suppression of neighboring class I crossovers can have opposite effects on effective interference depending on the distance between two genetic intervals.

INTRODUCTION

38
39
40
41
42
43
44

Meiotic crossovers shuffle parental genetic information generating new combinations of alleles. In most species the presence of one crossover inhibits nearby crossover formation so that the distances between crossovers are greater and more uniform, than if placed at random. This phenomenon, crossover interference, was first noted in genetic studies over a century ago

45 (1, 2), however it is only in the last few years that insights into its mechanistic basis have begun
46 to surface.

47

48 The inhibitory effect of interference is thought to spread a defined distance along the
49 chromosome axis, a linear proteinaceous structure formed by each chromosome at the base of
50 the chromatin loop array in early prophase (reviewed 3). By mid-prophase, homologous
51 chromosome axes are joined by additional proteins comprising the transverse filament and
52 central element to form the synaptonemal complex (SC). Although the interference signal
53 likely propagates prior to polymerization of the SC (3), the distance across which interference
54 spreads is usually specified in $\mu\text{m SC}$, as SC length is easier to measure cytologically and is
55 proportional to the length of the axis prior to synapsis. In yeast, interference is, at least in part,
56 mediated by Topoisomerase II (4) and wild type levels of interference require SUMOylation
57 of TopoII and the axis component Red1/Asy3 as well as ubiquitin-mediated removal of
58 SUMOylated proteins (4). These findings are consistent with suggested roles for the
59 chromosome axis and local stress relief via DNA remodeling, in mediating interference.

60

61 Several approaches have been used to model crossover (CO) patterning, the most notable being
62 the gamma model and the beam-film model. The gamma model is a statistical model based on
63 the observation that the distances between two crossovers are relatively uniform, following a
64 gamma distribution (5–7). Under this model “effective interference strength” is highest when
65 distances between crossovers show the least variation. This results in a large value of the
66 gamma shape parameter.

67

68 In contrast, the beam-film model is a mechanistic model whose various parameters have
69 biological correlates (8, 9). In the beam-film model, each bivalent has a number of precursor

70 sites (DSBs) that are subject to mechanical stress. CO designation at precursor sites is promoted
71 by stress and this stress is relieved locally following CO-designation. As stress promotes COs,
72 stress relief propagating out from crossover sites inhibits the formation of additional COs
73 nearby. In the beam-film model, interference strength is highest when stress relief propagates
74 furthest from designated crossover sites.

75

76 In most species, there are multiple crossover pathways. The majority of crossovers occur via
77 the interference sensitive class I pathway and are dependent on the ZMM group of proteins
78 identified initially in yeast (Zip1, Zip2, Zip3, Zip4, Mer3, Msh4, and Msh5) (10–17).
79 Crossovers occurring via this pathway are specifically marked by Zip3/Hei10 and MLH1 foci
80 at late pachytene (12, 18, 19). A number of secondary “clean-up” pathways repair DSBs not
81 metabolized by the class I pathway (20, 21). These clean-up pathways mostly repair DSBs as
82 non-crossovers, but also contribute a smaller number of crossovers (i.e. class II crossovers).
83 Class II crossovers are insensitive to interference (6, 22, 23) and usually make up 10-30% of
84 the total crossover number (e.g. 18, 22–24). In their simplest forms, the gamma and beam-film
85 models deal exclusively with class I crossovers and several studies have explored crossover
86 patterning in yeast using the single-pathway beam-film model (4, 9, 25, 26).

87

88 While the biological processes underlying meiosis and the various recombination pathways are
89 remarkably conserved across eukaryotes (27), differences in crossover patterning exist both
90 between and within species (27, 28). In *Arabidopsis* (29), as in many species (e.g. 30–33), there
91 are marked sex-specific differences in crossover patterning. Recombination rates are highest
92 in the male *Arabidopsis* germline, with particularly high levels of recombination in distal
93 regions (29). In contrast, distal regions have the lowest recombination rates in female (29).
94 Female meiosis has also been reported to have higher levels of interference (29). While these

95 differences have been repeatedly observed (29, 34), there has so far been little insight into the
96 biological factors contributing to them. Beam-film modelling offers an attractive means to
97 provide such insight, through estimating and comparing sex-specific values for the various
98 model parameters, each of which has a biological correlate.

99

100 Theoretically such analyses are possible from both genetic and cytological data. However,
101 while cytological analyses are routine in the Arabidopsis male germline, they remain
102 challenging for female meiosis. In addition, as the number of crossovers per chromosome is
103 low for female Arabidopsis, well over a thousand cells would need to be analyzed to achieve
104 the same number of inter-interval distances (the limiting factor for analyses) commonly
105 reported for yeast chromosomes (4, 9). For this reason, we took advantage of a previously
106 published large Arabidopsis reciprocal backcross recombination data set (~1500 individuals
107 and ~380 markers for both male and female) (29). Being genetically derived this dataset
108 comprised crossovers arising from both the class I and class II recombination pathways.

109 To identify likely biological determinants of sex-specific differences in Arabidopsis crossover
110 patterning we determined and compared sex-specific parameter values for various beam-film
111 model parameters. In addition, we comprehensively explored the behavior of the two-pathway
112 beam-film model, providing novel insights into how the patterning of class I and class II
113 crossovers interact to influence patterns of inheritance. Such insights have not been possible
114 from previous beam-film analyses focusing on the single-pathway model.

115

116 MATERIALS AND METHODS

117

118 **Experimental data:** Experimental dataset used has been previously published (29) and was
119 derived from large Arabidopsis reciprocal backcross populations. On average, 1,505 plants

120 were genotyped for 380 SNPs in the male population and 1,507 plants genotyped for 386 SNPs
121 in the female population (380 in common). As the average distance between markers is small
122 in this data set – 316 kb in male, 311 kb in female – the number of double crossovers (DCOs)
123 in a single interval are expected to be negligible (the average distance between DSBs is ~480
124 kb). It was therefore assumed during analysis that all recombination events were identifiable.
125 Genotyping and recombination datasets are provided (Datasets S1 and S2 respectively).

126

127 **Beam film parameter optimization:** Beam-film simulations were performed and best-fit
128 parameters determined using MADpatterns (25) and custom perl scripts with an approach
129 based on that described in (9). For each chromosome and each sex at least three rounds of
130 analysis were undertaken. In each round of each analysis 30,000 bivalents were simulated for
131 a range of parameter values. In the first round, to ensure the full parameter space was sampled,
132 relatively broad value ranges of optimised parameters (*Smax*: 2 - 10 L: 0.4 – 1.7; *T2Prob*: 0.002
133 - 0.008; *cL*: 0.3 - 1.3 and *cR*: 0.3 - 1.3) were chosen based on values described in Zhang et al
134 (2014) and comparison of ad hoc simulations with analysis of experimental datasets (35).
135 Parameters *N*, *B*, *E*, *Bs/Be/Bd*, *A* and *M* were set at appropriate default values (see below). In
136 the next two rounds, progressively smaller step-sizes between values were used to arrive at the
137 final parameter values. Descriptions of each parameter are provided below.

138 For each round of analysis, the crossover distributions, coefficient of co-incidence (CoC)
139 curves and event distributions (distribution of number of COs per gamete) simulated for each
140 chromosome were determined using MADpatterns (25) and compared to those obtained for the
141 relevant sex and chromosome from the experimental data set. For crossover distributions and
142 CoC curves, each chromosome was split into 13 equal sized adjacent intervals for analysis.
143 Importantly the experimental data are gamete data, while the MADpatterns program simulates
144 (and outputs) bivalent data (i.e. all crossovers on a pair of homologous chromosomes).

145 Therefore, all simulated bivalent crossover frequencies were halved to convert to gamete
146 crossover frequencies. Bivalent event distributions were also converted to gamete event
147 distributions, assuming random assignment of each crossover to two of the four chromatids i.e.
148 each crossover has a 50% chance of being inherited by a gamete arising from that meiosis.
149 Parameter sets were ranked based on the difference between simulated and experimentally
150 determined CoC distributions [$\text{Score}_{\text{CoC}} = \sum_{\text{IID}} \text{abs}(\log_2(\text{CoC}_{\text{sim}}/\text{CoC}_{\text{exp}}))$], CO distributions
151 [$\text{Score}_{\text{CO}} = \sum_{\text{Int}} (\text{CO}_{\text{sim}} - \text{CO}_{\text{exp}})^2$] and event distributions [$\text{Score}_{\text{ED}} = \sum_{\text{Enum}} (\text{ED}_{\text{sim}} - \text{ED}_{\text{exp}})^2$].
152 Simulations were ranked for each score and final parameter values chosen were those with the
153 lowest rank-sum. For graphical representation, CoC curves were smoothed using locally
154 estimated scatterplot smoothing (LOESS, span 0.3-0.5).

155

156 **Optimized Parameters:** Beam-film model parameters S_{max} , L_{BF} , cL/R and T2Prob were
157 optimized (see above). Parameters N , B , E , $B_s/B_e/B_d$, A and M were fixed based on known
158 values of the biological correlates, parameters that tend to be stable between species (9), or
159 suggested default values (36). A description of each of these parameters is given below, further
160 explanations can be found in refs. (9, 25).

161

162 **Beam-film Parameters**

163 The beam-film program requires three kinds of parameters: 1) precursor array parameters,
164 which determine the position and number of potential crossover sites (DSBs) along each
165 bivalent, 2) crossover patterning parameters, that determine which precursor sites become
166 designated crossover sites and 3) the maturation efficiency parameter which determines the
167 likelihood of designated crossover sites maturing to become true crossovers.

168

169 **Precursor Array Parameters:**

170 *N – Precursor sites per bivalent:* Parameter N sets the number of potential recombination sites
171 or “precursors” on a bivalent. The biological correlate is the number of meiotic DSBs for that
172 bivalent. For the first round of simulations we assumed 250 DSBs per meiosis in both male
173 and female. For any given chromosome N was set to $250 \times$ proportion total genome size (in
174 Mb) contributed by that chromosome. For modelling of reduced DSB formation in female N
175 we calculated as above assuming 150 DSBs genome wide.

176

177 *B – Similarity in total precursor number between bivalents:* B sets the similarity of precursor
178 number between the multiple bivalents simulated for a given chromosome in each round of
179 analysis. Precursor number for any given chromosome was set to be constant for each bivalent
180 simulated ($B = 1$).

181

182 *E – Evenness of precursor spacing:* There is considerable experimental evidence that DSB
183 spacing is non-random, being more evenly spaced than if placed at random (37, 38). For
184 numerous organisms a parameter value of 0.6 has been found appropriate (9) and we therefore
185 set E to 0.6 for all simulations (0 = random, 1 = even).

186

187 *A – Intrinsic precursor sensitivities:* In the early steps of the model each precursor is assigned
188 a “sensitivity”, reflecting the fact that not all DSBs have an equal chance of becoming a
189 crossover; local factors e.g. SNP density, local structural diversity, epigenetic landscape may
190 also influence the fate of each precursor site. Parameter A determines how precursor
191 sensitivities are assigned. For all simulations A was set to 1 – sensitivities assigned from a
192 uniform distribution.

193

194 *Bs/Be/Bd* – Recombination “black hole” start/end/precursor density: Recombination black
195 hole start (*Bs*) and end (*Be*) points delineate the start and end of the heterochromatic
196 centromeric region which has reduced DSB formation. Parameter *Bd* indicates the relative
197 precursor density of the “black hole” and was set to 0.01 for all simulations (1 = no reduction
198 in precursors, 0 = no precursor formation). Values were determined based on recombination
199 frequencies observed in the backcross data (Table S1, Figure S1) and correspond to regions of
200 the Arabidopsis genome with high DNA methylation, low H3K4me3, and reduced DSB
201 formation (38).

202

203 **Crossover Patterning Parameters:**

204 *Smax* - Maximum stress level per bivalent: Crossovers are promoted at precursor sites by
205 crossover promoting “stress” (*S*). *Smax* is maximum level of stress a bivalent is subject to
206 during simulation. The biological correlate of the crossover promoting stress is not precisely
207 defined but may relate to the expansion of chromatin during early prophase (8).

208

209 *Bsmax* – Similarity in maximum stress levels between bivalents: *Bsmax* sets the similarity of
210 *Smax* between simulated bivalents and was set to be constant for all simulations (*Bsmax* = 1).

211

212 *L_{BF}* – Stress relief distance: The parameter *L_{BF}* corresponds to the length of the chromosomal
213 interval over which a CO relieves stress i.e. stress-relief propagates out from COs a distance of
214 $\frac{1}{2} L_{BF}$ in either direction.

215

216 *cL/R* – Left and Right end clamping: In the beam-film model, “clamping” at chromosome ends
217 determines how stress is supported in terminal regions. Unclamped chromosome ends (*cL* = 0;
218 *cR* = 0) cannot support stress and so locally relieve stress, behaving as if there were a crossover

219 at the chromosome end. Clamped chromosome ends ($cL = 1$; $cR = 1$) experience stress as
220 elsewhere along the bivalent.

221

222 *T2Prob* - Probability that a non-crossover designated precursor will form a Type II crossover:

223 The parameter *T2Prob* defines the probability that a precursor site (i.e. DSB) not designated to
224 become a class I crossover will become a class II crossover.

225

226 **Maturation Parameter:**

227 *M* – Crossover maturation efficiency: In the beam film model, it is possible to model failure of
228 crossover maturation. If failure occurs, the CO-designated site inhibits nearby crossovers but
229 does not itself develop into a crossover. We assumed 100% crossover maturation efficiency
230 for all simulations ($M = 1$).

231

232 **Double crossover class determination:** The proportion of each class of DCO for a given inter-
233 interval distance was determined from simulations modelling the formation of class I
234 crossovers only ($T2Prob = 0$), class II crossovers only ($Smax = 0$), or both class I and II
235 crossovers. For each simulation, numbers of DCOs were tallied for each inter-interval distance
236 (IID, the distance between a pair of genetic intervals). For each IID, numbers of DCOs
237 involving two class I COs (DCO_{I_I}), two class II COs ($DCO_{II_{II}}$) or all DCOs (DCO_{ALL}) were
238 calculated from the respective simulations. $DCO_{I_{II}} = DCO_{ALL} - (DCO_{I_I} + DCO_{II_{II}})$.

239

240 **Response of model to parameters *L*, *Smax*, *T2Prob* and *N*:** To investigate the response of
241 the model to parameters *L*, *Smax* and *T2Prob* we simulated 30000 bivalents for an “idealized”
242 male Arabidopsis chromosome ($N = 60$, $B = 1$, $E = 0.6$, $Bs = 0.45$, $Be = 0.55$, $Bd = 0.01$, *Smax*

243 = 9, $B_{smax} = 1$, $A = 1$, $L = 0.7$, $cL = 0.8$, $cR = 0.8$, $M = 1$, $T2Prob = 0.004$) as described above,
244 varying one specified parameter.

245

246 **Data availability statement**

247 Dataset S1 contains male and female genotyping data originally reported in Girault et al. (29).

248 Dataset S2 contains male and female recombination location data. Code used for parameter

249 optimization is available at <https://github.com/andrewhmlloyd/BeamFilmBestFit>.

250

251

RESULTS

252 **Beam-Film simulations replicate CO patterning in Arabidopsis.**

253 To determine the likely biological determinants of differences in crossover patterning between

254 male and female meiosis, we compared beam-film parameter estimates obtained for the two

255 sexes. To obtain these estimates, we ran a series of beam-film simulations using a broad range

256 of parameter values and compared simulated recombination data to our experimental dataset.

257 Independent simulations were run for each of the five Arabidopsis chromosomes for each sex.

258 Parameter best-fits for each chromosome and sex were then obtained by comparing crossover

259 number and distribution, and interference relationships (CoC curves) of simulated

260 recombination and experimental data (Figure 1 & S1-2). Global parameter estimates were then

261 derived for male and female meiosis by averaging the individual estimates of the five

262 chromosomes (Figure 2). As parameter estimates for male and female are drawn from the same

263 parameter space, the female best-fit simulations are an example of a parameter set that did not

264 fit the male data and vice versa. Figure S3 shows several other examples.

265

266 **Crossover Distribution:** Simulated CO distributions using optimized parameter sets

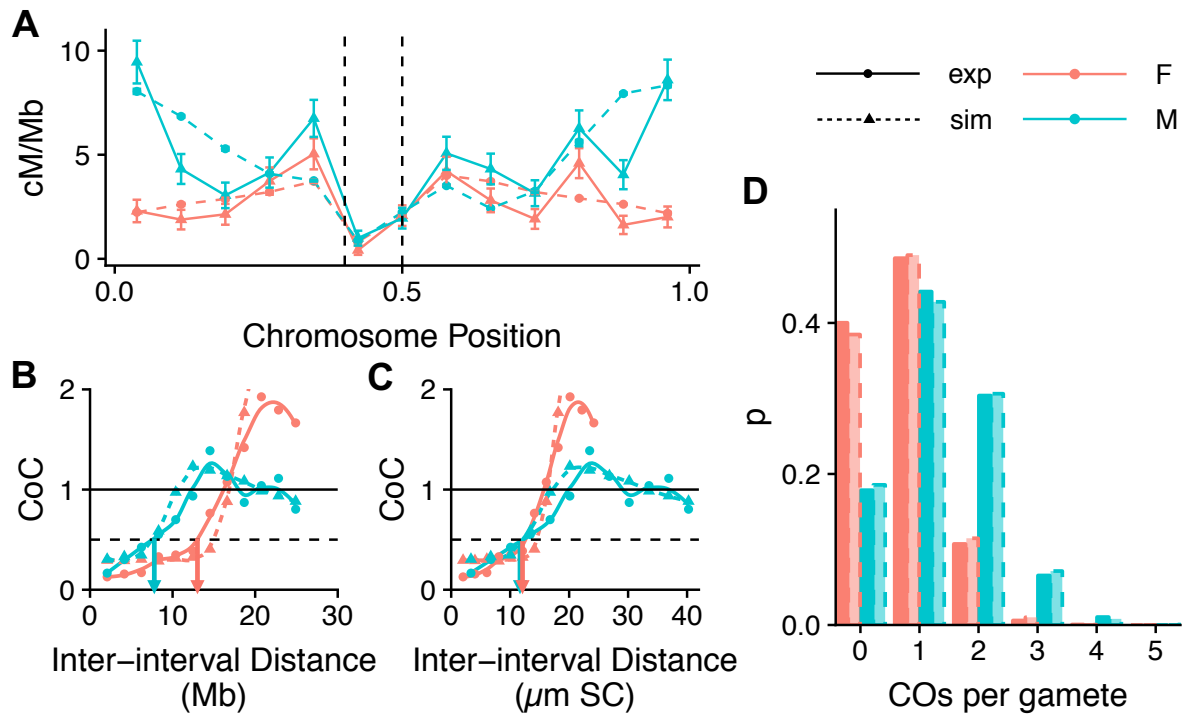
267 reproduced CO distributions observed in the experimental data. Simulations captured the broad

268 scale trends, rather than fine-scale differences in CO frequency. Highest recombination in
269 males was found in distal regions and highest recombination in females in regions adjacent to
270 the centromere (Figure 1, Figure S1). The exception was the short arms of chromosomes 2 and
271 4 in males which have high experimental recombination rates but had low levels of
272 recombination when simulated using the global best-fit parameters (Figure S1). It is possible
273 that this is related to the presence of nucleolar organizer regions (NORs) on the short arms of
274 these two chromosomes, which are not explicitly modelled in simulations.

275 **CoC curves:** The coefficient of coincidence (CoC) is the ratio of the observed and expected
276 numbers of double crossovers (DCOs) for a given pair of intervals, given the rates of single
277 COs in the two intervals. When interference strength is high, CoC values tend to be low as
278 there are fewer DCOs observed than expected. CoC shows a characteristic curve when plotted
279 against inter-interval distance (Figure 1B-C), with low CoC for small inter-interval distances
280 (when a CO in one interval suppresses the occurrence of a CO in the neighboring interval) and
281 CoC approximating 1 for large inter-interval distances (over which the interference signal no
282 longer spreads along the chromosomes). A useful measure when analyzing such curves is L_{CoC}
283 (9), the inter-interval distance at which the observed number of double crossovers is half the
284 expected number (CoC = 0.5, dashed line, Figure 1B-C). For all analyses the simulated data
285 gave L_{CoC} values that were no different from those determined from the equivalent
286 experimental data (Table 1.). For both experimental and simulated data, L_{CoC} was significantly
287 smaller in males than in females if measured in Mb but showed no difference when measured
288 in μm SC (Table 1, Figure 1 and Figure S2). This confirms that genetic measurements of
289 interference (e.g. L_{CoC} in Mb) are lower in male than in female but suggests that the physical
290 distance over which interference spreads (measured in μm SC) may be similar.

291

292 In the Beam film model, the CO patterning process is primarily determined by the strength of
 293 the (CO)-designation (S , S_{max}) and by the distance over which interference spreads (L_{BF}). We
 294 thus compared estimates of these two parameters between male and female meiosis.
 295
 296



297
 298 **Figure 1. Crossover analysis for Arabidopsis chromosome 5.** Each analysis includes experimental
 299 (solid lines) and simulated (dashed lines) data for male (blue) and female (orange). **A** Crossover
 300 distributions for Arabidopsis chromosome 5. Dashed lines represent the limits of the centromeric region
 301 over which precursor (DSB) number is markedly reduced both biologically (38) and during simulations.
 302 Error bars indicate 95% confidence intervals. **B-C** CoC curves for chromosome 5 with inter-interval
 303 distance (IID, the distance between a pair of genetic intervals) measured in Mb (**B**) or $\mu\text{m SC}$ (**C**). L_{CoC}
 304 for male and female (blue and orange arrows respectively) differed when IIDs were measured in Mb
 305 but not when measured in $\mu\text{m SC}$. **D** Event distribution for chromosome 5. Male and female simulations
 306 shown, assume 250 DSBs genome-wide. Chromosomes were divided into 13 equal-sized adjacent
 307 intervals for analysis.
 308

309 **Estimates of crossover promoting “stress” are the same for male and female meiosis**

310 In the beam-film model precursor (DSB) fate is determined by the crossover-promoting
311 “stress” (S) experienced by that precursor as well as the precursor’s sensitivity (a random value
312 between 0-1, determined by parameter A , see methods). When simulating each bivalent, the
313 value of S is progressively increased until $S = S_{max}$, with each precursor experiencing stress
314 equal to the product of S and the precursor’s sensitivity. At some point the stress experienced
315 by the most sensitive precursor reaches the critical value of 1 and will undergo CO-designation.
316 Stress-relief will then extend out from that position. As S increases to S_{max} , additional
317 precursors usually experience sufficient stress to promote the designation of further COs,
318 although in these subsequent rounds of crossover designation, the stress experienced by
319 precursors is reduced by the sum of any stress-relief caused by interference from nearby COs.
320 If S_{max} is set below 1 then no pre-cursor will achieve the critical stress value and therefore no
321 class I crossovers will be designated.

322

323 According to this model, the higher the final maximum stress value (S_{max}), the more CO-
324 designations. However, despite male having significantly more COs than female, the predicted
325 levels of maximum stress for the five chromosomes were similar for both sexes: S_{max} - male
326 7 ± 1.9 and female 6.9 ± 0.7 , $p = 1$ (Bonferroni corrected) (Figure 2, Table S1). Thus, our
327 modelling suggests that increased crossover frequencies in male are not due to differences in
328 the CO-designation driving force.

329

330 **Interference propagates the same physical distance along male and female bivalents, but**
331 **has a greater “effective” strength in female.**

332 The parameter L_{BF} determines the length of the chromosomal region, centered on a crossover,
333 over which stress is relieved by that crossover. In the beam-film model, the magnitude of the

334 stress-relief decreases exponentially with distance from the CO, such that there is maximal
335 stress-relief immediately surrounding the CO and almost no stress-relief at a distance $\frac{1}{2} L_{BF}$ in
336 either direction from the CO (8, 9).

337 When running simulations L_{BF} is specified as the proportion of total chromosome length (i.e.
338 chromosome length is set to 1), but is converted to length in Mb or μm SC to enable
339 comparisons between chromosomes of different lengths. For some chromosomes, the
340 estimated distance over which stress is relieved was greater than the length of the chromosome
341 in question. While this may at first seem contradictory, it is in fact required if a CO suppresses
342 the formation of additional COs more than half the length of the chromosome away. An
343 example can be seen for chromosome 2 in females which has an estimated SC length of 16.2
344 μm and an estimated stress relief distance (L_{BF_SC}) of 25.9 μm . As can be seen from the CoC
345 curve for this chromosome (Figure S2) it is clear that the observed number of DCOs are less
346 than expected (i.e. CoC < 1) even when intervals are at opposite ends of the chromosome (e.g.
347 inter-interval distance $\sim 14 \mu\text{m}$).

348 When measured in Mb (L_{BF_Mb}) the average best-fit estimates of stress relief distance were
349 significantly higher in females: L_{BF_Mb} – male 17.1 ± 3.5 Mb and female 28.8 ± 3.1 Mb, $p =$
350 0.0095 Bonf. corr. (Figure 2, Table S1). However, when the distance metric was converted to
351 μm SC (L_{BF_SC}), using the best available estimates of SC length in the two sexes (39), there
352 was no-longer any difference in the estimated stress relief distance between the two sexes:
353 L_{BF_SC} – male $27.7 \pm 5.6 \mu\text{m}$ and female $23.7 \pm 2.5 \mu\text{m}$, $p = 1$ Bonf. corr. (Figure 2). These
354 results indicate that the physical distance over which interference spreads is the same in both
355 male and female, but that the effect of interference on patterns of inheritance is greater in
356 female than it is in male. This is because the same physical distance (μm SC) covers a greater
357 proportion of total chromosome length (Mb) in female.

358 These findings highlight a key distinction between different possible interpretations of
359 interference that can be broadly defined as “mechanistic” and “effective”. For clarity we here
360 define our use of these terms which we will use in the remainder of this manuscript: We use
361 the term “interference” when speaking broadly of the phenomenon, we use “mechanistic
362 interference” when referring specifically to interference as defined in the beam-film model i.e.
363 the distance along the chromosome (measured in $\mu\text{m SC}$) that the interference signal
364 propagates, and we use the term “effective interference” to refer to interference as measured
365 genetically (e.g. CoC or gamma, calculated from genetic data and expressed in Mb). “Effective
366 interference” can be influenced by stress relief distance (in $\mu\text{m SC}$), but is also affected by
367 other factors like rates of class II crossovers and chromatin loop size (Mb per $\mu\text{m SC}$). Thus,
368 although mechanistic interference is identical for male and female meiosis, effective
369 interference is stronger in female, resulting in fewer interference sensitive class I COs in
370 female.

371

372 **Estimates of chromosome end tethering (cL/R) are the same for male and female meiosis**

373 In addition to S_{max} and L_{BF} , several other beam-film parameters commonly vary within or
374 between species, and might contribute to sex-specific patterns of crossover formation (9). The
375 first of these we focused on was the effect of “clamping” or tethering of chromosome ends,
376 which determines how stress is supported in terminal regions. A probable biological correlate
377 is the tethering of telomere ends to the nuclear envelope. If a chromosome is clamped/tethered
378 it can support crossover promoting stress. If unclamped, stress can dissipate from the loose
379 chromosome end which, according to the beam-film model, would tend to suppress CO
380 formation. As the interference signal (stress-relief) cannot come from beyond the end of the
381 chromosome, recombination frequencies will tend to be highest in distal regions when
382 chromosomes are clamped and there is more than one CO per bivalent. Total clamping

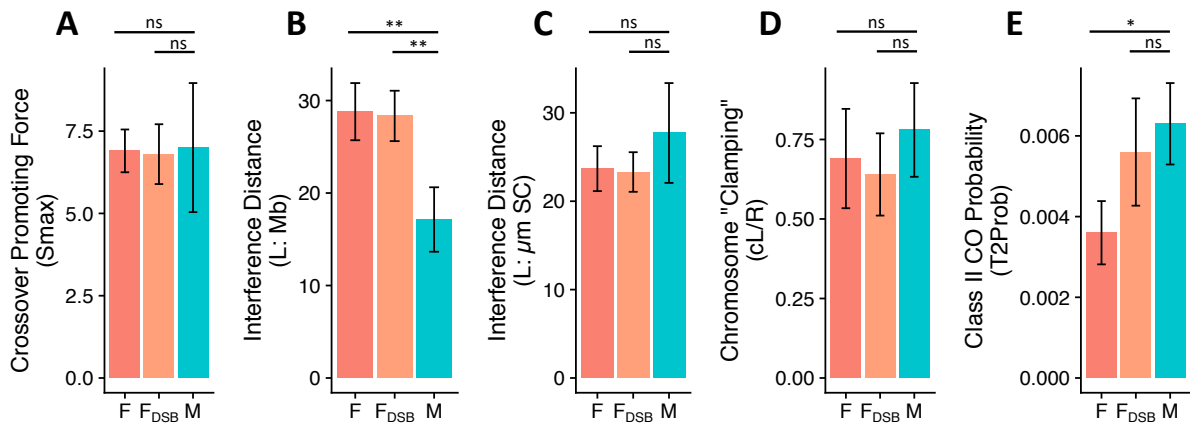
383 averages (cL/R) for male and female were calculated from the estimated values of cL and cR
384 for each sex. Clamping values were variable between chromosomes but there was no
385 significant difference between the average clamping values: cL/cR male 0.78 ± 0.16 and female
386 0.69 ± 0.13 , $p = 1$ Bonf. corr. (Figure 2). Differences in chromosome-end tethering are therefore
387 unlikely to contribute to sex-specific differences in crossover patterning.

388

389 **Fewer class II crossovers occur through the female germline**

390 The number of class II COs in a simulation is determined by parameter N , the number of
391 recombination precursor sites (DSBs) and parameter $T2Prob$ which specifies the probability of
392 a non-crossover designated precursor site becoming a class II CO. Assuming the same number
393 of DSBs in male and female, the estimated likelihood of precursors becoming a class II CO
394 was significantly higher in male than female meiosis: $T2Prob$ - 0.0063 ± 0.0010 and $0.0036 \pm$
395 0.0008 respectively ($p = 0.026$, Bonf. corrected, Table 1, Figure 2). As male and female meiosis
396 have the same number of precursors (DSBs) in these analyses, males have a proportionately
397 higher number of class II COs: 1.575 ± 0.5 and 0.9 ± 0.2 respectively ($p = 0.026$, Bonf.
398 corrected). We also determined what proportion of the total number of crossovers occur via the
399 class II pathway (i.e. $p = CO_{II} / (CO_I + CO_{II})$). These values were equivalent for the two sexes:
400 0.14 ± 0.02 male, 0.14 ± 0.03 female, $p = 1$ Bonf. corr. A lower probability of class II crossover
401 formation in female may therefore, in addition to the decrease in class I crossovers described
402 above, contribute to sex-specific crossover patterning in Arabidopsis.

403



404

405 **Figure 2. Beam-film best-fit parameter estimates.** **A)** Estimates of crossover promoting force (S_{max}) were
 406 identical for male and female with 250 DSBs (M and F respectively), and female with 150 DSBs (F_{DSB}).
 407 Estimates of interference distance (L) were longer in male when measured in Mb (**B**) but not significantly
 408 different when measured in $\mu\text{m SC}$ (**C**). **D)** There was no significant difference in estimates of chromosome
 409 clamping. **E)** The probability of non-class I-designated precursors becoming class II crossovers was
 410 estimated to be lower in female than male if both sexes had 250 DSBs, but not significantly different if there
 411 are reduced DSBs (150) in female. For each parameter and condition, the mean of the estimates for the five
 412 chromosomes is shown. Error bars indicate 95% confidence interval. * $p < 0.05$, ** $p < 0.01$, after Bonferroni
 413 multiple comparison correction.

414

415 **Fewer DSBs in female would explain lower class II CO numbers and unify estimates of**
 416 **beam-film parameters for male and female meiosis.**

417 One of the parameters fixed for each round of analysis is the number of DSBs. While there are
 418 relatively good estimates for the number of DSBs in male meiosis in Arabidopsis, cytological
 419 analyses of female meiosis are more challenging and there are no reliable estimates of DSB
 420 numbers. Thus, while we have assumed equal numbers of DSBs in male and female meiosis in
 421 the analyses described above, it is possible that DSB numbers differ between the two sexes.
 422 Meiotic DSBs occur in loop DNA that has been recruited to the chromosome axis (40). In
 423 Arabidopsis female meiosis there are fewer (albeit larger) chromatin loops and the
 424 chromosome axis is 40% smaller than in male meiosis (39) which could feasibly result in a

425 similar reduction in DSBs (31, 41). To understand whether reduced DSB numbers would have
 426 any effect on crossover patterning and/or estimates of parameter values in female meiosis, we
 427 repeated the best fit simulations assuming a reduction in DSBs equal to the reduction in SC
 428 length i.e. approx. 40% reduction, or 150 (rather than 250) DSBs per meiosis.

429

430 Optimized estimates of crossover promoting stress (S_{max}), interference strength / stress relief
 431 distance (L_{BF_Mb} , L_{BF_SC}) and chromosome tethering (cL/cR) were identical for both sets of
 432 simulations (F and F_{DSB} , Figure 2). Estimates of class II crossover likelihood ($T2Prob$) were
 433 higher for simulations of female meiosis with reduced DSB numbers, and the optimized value
 434 no-longer differed from that estimated for male meiosis (Figure 2). Although the probability
 435 of class II CO formation was the same for male with 250 DSBs and female with 150 DSBs, the
 436 absolute number of class II crossovers was lower in female (due to the reduced number of
 437 DSBs): Male - 250 DSBs $\times T2Prob$ $0.0063 \pm 0.001 = 1.58 \pm 0.25$; Female - 150 DSBs $\times T2Prob$
 438 $0.0056 \pm 0.001 = 0.90 \pm 0.17$ COs.

439

440

Table 1. L_{CoC} values

	Mb			$\mu\text{m SC}$		
	male	female	p value [#]	male	female	p value [#]
experimental	7.05 \pm 0.50	12.84 \pm 1.50	7.90E-07	11.65 \pm 0.86	12.83 \pm 1.50	1
simulated	6.30 \pm 1.05	11.60 \pm 0.83	1.40E-05	10.21 \pm 1.75	11.20 \pm 0.78	1
p value [#]	1	1		1	1	

[#]Bonferroni multiple-comparison corrected

441

442 Taken together, these results suggest that the smaller synaptonemal complex length in female,
 443 if accompanied by an equivalent reduction in DSBs, can account for all differences in crossover
 444 patterning between the two sexes, even if the mechanics of crossover patterning remain
 445 identical. The smaller SC in female accounts for stronger effective interference, and therefore

446 reduced crossovers, despite identical estimates of L_{BF_SC} . Similarly, a reduction in DSB density
447 (per Mb), due to the shorter SC, could account for the reduction in class II crossovers.

448

449 **Behavior of two-pathway beam-film model**

450 We next comprehensively explored the behavior of the two-pathway beam-film model, in order
451 to better understand how the patterning of class I and class II crossovers interact to influence
452 patterns of inheritance. To do this we simulated crossovers, independently varying the stress
453 relief distance (L_{BF} , Figure 3A-C), crossover promoting stress (S_{max} , Figure 3D-F) and class
454 II CO probability (T2Prob, Figure 3G-I).

455

456 **COs tend to increase in regions adjacent to telomeres and pericentromeres**

457 Changes in L_{BF} and S_{max} dramatically altered CO distributions (Figure 3A & 3D) while
458 changing the proportion of class II COs had little effect (Figure 3G). Changes in CO frequency
459 were primarily observed in terminal regions (S_{max} , L_{BF}) and in regions adjacent to the peri-
460 centromere (L_{BF}) and showed increased CO frequencies with greater stress and decreased stress
461 relief distance (Figure 3A & 3D).

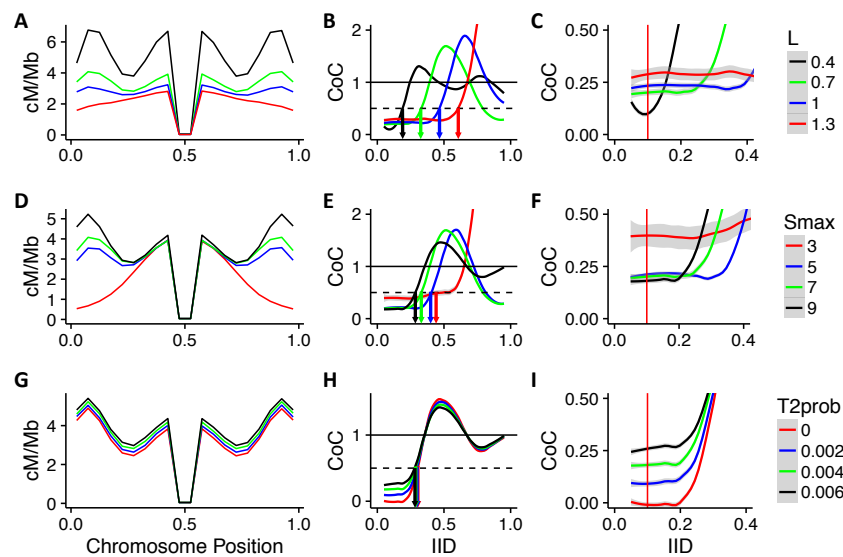
462

463 **L_{CoC} is primarily influenced by stress relief distance**

464 As has been observed previously in yeast (9) the parameter that most influenced CoC curves
465 was the stress relief distance (L_{BF}) with higher values of L_{BF} shifting CoC curves to the right.
466 Because of this shift, increases in L_{BF} resulted in proportional increases in L_{CoC} , highlighting
467 that L_{CoC} (when measured in μm SC) is a useful proxy for stress relief distance. One major
468 advantage of L_{CoC} over L_{BF} is that it can be determined directly from experimental data without
469 the requirement for beam-film modelling and parameter optimization.

470 Intriguingly, behavior of CoC at small inter-interval distances differed from that observed at
 471 larger inter-interval distances. For example, an increase in the distance over which the
 472 interference signal is propagated would normally be expected to lead to lower values of CoC
 473 as more double crossovers are suppressed. However, at small inter-interval distances increased
 474 L_{BF} resulted in *increased* values of CoC (Figure 3C). It was also evident that while changes in
 475 the probability of class II CO formation had negligible effects on L_{CoC} and the shape of the CoC
 476 curve, it was the parameter that had the largest impact on CoC at small inter-interval distances
 477 (IID ~ 0.1 , red lines, Figure 3I vs Figures 3C and 3F).

478



479

480 **Figure 3. Effect of beam-film parameters on crossover patterning in Arabidopsis.** The effect of altering
 481 a single beam film parameter – L (A-C), Smax (D-F) or T2Prob (G-I) – on crossover distribution (A, D &
 482 G) and CoC (B-C, E-F and H-I). Red vertical lines in C, F and I represent IID = 0.1. Grey shading in CoC
 483 curves indicate 95% confidence interval.

484

485 **Differing classes of double COs at small and large IIDs cause opposite effects of altered**
 486 **stress relief distance on CoC:** To further understand why CoC might behave differently at
 487 different inter-interval distances (IIDs), we sought to identify how changes in L_{BF} might
 488 differentially affect the expected and observed number of double COs (the determinants of

489 CoC) for different IIDs. Beam film simulations demonstrated that increased L_{BF} resulted in a
490 small decrease in the expected number of double COs (DCOs) for both small and large IIDs
491 (IID = 0.1 and 0.5; Figure 4A). This was anticipated given that the expected number of DCOs
492 for a pair of intervals is based purely on the respective rates of COs in the two intervals. In
493 contrast, the observed number of DCOs changed dramatically for IID = 0.5, but only
494 marginally for IID = 0.1 (Figure 4A) in response to changes in L_{BF} . As a result, CoC
495 dramatically decreased for IID = 0.5 with increased L_{BF} but increased slightly for IID = 0.1
496 (Figure 4B).

497

498 We reasoned that the difference in behavior might be due to the nature of the DCOs formed at
499 smaller and larger IIDs which might differ in their sensitivity to interference. For example,
500 DCOs can occur between two class I COs, two class II COs or between a class I and a class II
501 CO but interference only directly suppresses those involving two class I COs. We therefore ran
502 beam film simulations with class I COs only ($T2Prob = 0$), class II COs only ($Smax = 0$), or
503 both class I and class II COs and determined numbers of the different classes of DCOs formed
504 for each set of simulations at different IIDs (Figure 4C). From these numbers we determined
505 the proportions of the different classes of DCOs (Figure 4D) that occur for different IIDs under
506 standard conditions (i.e. when simulating both class I and class II COs). For small IIDs DCOs
507 are almost exclusively formed between a class I CO and a class II CO (Figure 4D). In contrast,
508 for larger IIDs (≥ 0.4) the majority of DCOs are formed between two class I COs (Figure 4D).
509 Cytological observations in tomato reporting the same phenomenon (42) suggest this is a
510 general feature of meiosis. As interference only suppresses DCOs involving two class I COs,
511 changes in L_{BF} will only directly affect DCO formation at larger IIDs. This pattern holds when
512 the proportion of class II crossovers falls within the range normally observed (5-20%), although

513 when class II crossovers are absent or make up the majority of crossovers then most DCOs
 514 involve two class I or two class II COs respectively for all IIDs (Figure S4).

515

516 Both the expected number of DCOs and observed DCOs at small IIDs are indirectly affected
 517 by increased L_{BF} due to the associated decrease in the frequency of class I COs. The magnitude
 518 of the change is greater for the expected number of DCOs, which can be seen from the
 519 equations below. Here CI and CII are the rates of class I and class II crossovers respectively in
 520 the two intervals:

$$521 \quad DCO_{exp} = (CI_{Int1} + CII_{Int1}) \times (CI_{Int2} + CII_{Int2})$$

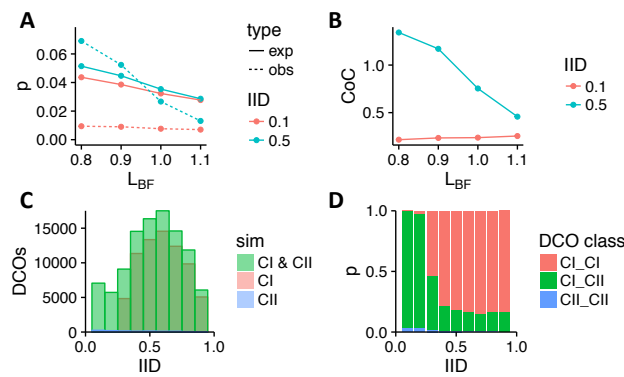
522

$$523 \quad DCO_{obs_{small_IID}} \sim (CI_{Int1} \times CII_{Int2}) + (CI_{Int2} \times CII_{Int1})$$

524

525 For small IIDs, while $CI \gg CII$, the reduction in the expected number of DCOs is
 526 approximately twice that of the observed reduction in DCOs, resulting in an increase in CoC.

527



528

529 **Figure 4. Influence of IID on CoC response to changes in L_{BF} .** **A** The expected (solid line) and observed
 530 (dashed line) proportion of interval pairs receiving a double crossover (DCO) for two different inter-interval
 531 distances (IIDs); calculated from simulations with varying values of L_{BF} . **B** CoC values for two IIDs
 532 calculated from simulations with varying values of L_{BF} . **C** The number of DCOs observed for different IIDs
 533 from simulations involving class I and class II crossovers (CI & CII), class I crossovers only (CI) or class II

534 crossovers only (CII). **D** The proportions of DCOs formed between two class I crossovers (CI_CI), two class
535 II crossovers (CII_CII), or a class I and a class II CO (CI_CII) for different IIDs.

536

537 **Crossover homeostasis is influenced by the proportion of class II COs:**

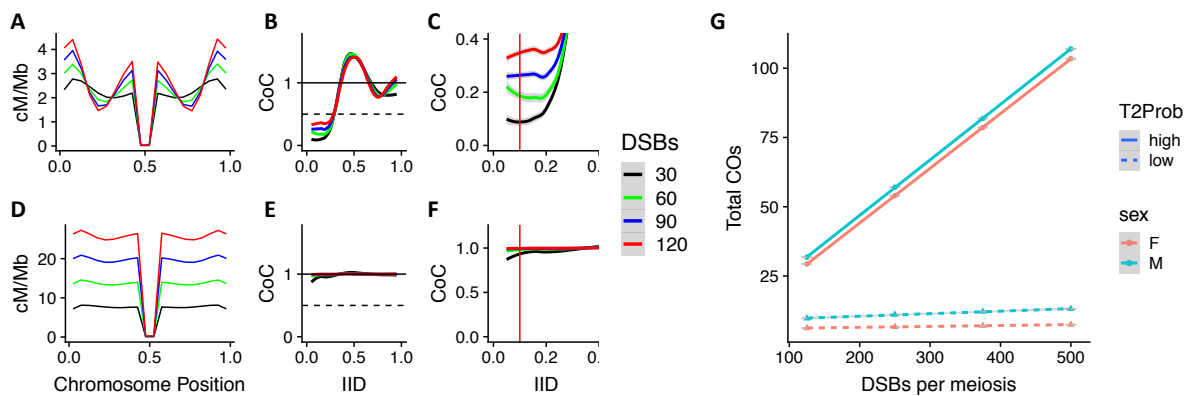
538 Finally, we assessed the effects of the rate of class II crossover formation on crossover
539 homeostasis. Crossover homeostasis maintains crossover number despite differences in DSB
540 formation (43–45). As described above, we observed few changes in crossover number and
541 estimates of beam-film parameters when we modelled a 40% decrease in DSB numbers, the
542 beam-film model therefore displays strong CO homeostasis when modelling wild type
543 Arabidopsis meiosis. We reasoned however, that if the proportion of class II crossovers
544 increased, such as is seen in some mutant contexts (e.g. 34), then DSB number should have a
545 greater influence on the number of crossovers.

546

547 When modelling wild type meiosis, altered DSB number had relatively little effect on crossover
548 distributions or CoC curves (Figure 5A-B). For CO distribution, increased DSBs resulted in a
549 slight increase in proximal and distal crossovers, but fewer interstitial crossovers. The only
550 clear difference in CoC was for small inter-interval distances, where higher DSB numbers
551 resulted in higher values of CoC (Figure 5C). In contrast, altering the number of DSBs in a
552 context where a high proportion become class II crossovers had a dramatic effect on crossover
553 patterning. Here increased DSBs resulted in proportionate increases in crossovers (Figure 5D).
554 Regardless of the number of DSBs, CoC values were approximately 1 for all inter-interval
555 distances (Figure 5E-F).

556 We next modelled how DSB number affects the total number of crossovers for male and female
557 meiosis in both contexts. In wild type, doubling the number of DSBs resulted in a ~ 15%
558 increase in crossovers in male and female (Figure 5G). In a context with a high number of class
559 II crossovers, doubling the number of DSBs resulted in almost doubling the number of

560 crossovers (Figure 5G). The number of DSBs has often been reported to have limited influence
 561 on rates of crossovers due to crossover homeostasis (43–45). Our results indicate that the
 562 number of DSBs primarily affects the number of COs when the proportion of class II crossovers
 563 is high, and by extension suggests that the probability of class II CO formation has a major
 564 influence on crossover homeostasis.
 565 For a given number of DSBs the modelling predicts ~ 65% more crossovers in wild type male
 566 than wild type female, but essentially equal numbers of crossovers when the probability of
 567 class II crossovers is high (Figure 5G).
 568



569

570

571 **Figure 5. Influence of DSB number on crossover patterning and homeostasis is dependent on the**
 572 **probability of class II crossovers. A-C** show results for simulations of wild type meiosis, **D-F** show results
 573 for simulation of meiosis with increased class II crossover formation (T2Prob). **A)** Increased DSBs in wild
 574 type resulted in more proximal and distal crossovers, but fewer interstitial crossovers. **D)** In mutants with
 575 increased class II crossovers, more DSBs resulted in a uniform increase in crossovers. **B-C)** For wild type ,
 576 CoC values increased at small inter-interval distances with increased DSBs. **E-F)** With increased class II
 577 COs, CoC values were ~1 for all inter-interval distances and all DSB numbers. **(G)** Total crossover number
 578 for genome-wide simulations using best-fit parameters for male and female meiosis and varying numbers of
 579 DSBs. In wild type (dashed lines) increasing DSBs had a minimal effect on total crossovers. With increased
 580 class II COs (solid lines) doubling DSBs resulted in twice as many crossovers. Grey shading in CoC curves
 581 indicates 95% confidence interval.

582

583

DISCUSSION

584 Crossover interference is a well-known genetic phenomenon; however, its mechanistic basis is

585 only just now coming to light. The interference signal is thought to propagate a set physical

586 distance (L_{BF} , usually measured in $\mu\text{m SC}$) from designated crossover sites (4, 9), and analyses

587 commonly use cytological observations and simulations of class I crossover positions along

588 the length of a synapsed bivalent (4, 9).

589

590 To gain insights into the differences between female and male meiosis in Arabidopsis, we

591 analyzed a large Arabidopsis reciprocal backcross data set (29) and performed two-pathway

592 (i.e. both class I and class II COs) beam film best-fit simulations. Our modelling suggests that

593 the major differences in crossover number, crossover distribution and interference relationships

594 between the sexes can all be explained by the observed difference in SC length between male

595 and female meiosis. The relationship between genome size and SC length is governed by the

596 size/number of chromatin loops, which occur at a conserved density of ~ 20 per $\mu\text{m SC}$ across

597 a wide range of organisms (46). As genome size is identical for both sexes in Arabidopsis, we

598 would expect loop size in male meiocytes to be about 60% of that found in female meiocytes.

599 Exactly how chromatin loop size is determined remains unclear but this decision occurs very

600 early in, or prior to, meiosis (3, 47). It is probable, therefore, that the cause of differences in

601 crossover patterning also occurs very early in, or prior to, meiosis. Interestingly humans also

602 display a sex-specific differences in chromatin loop-size and SC length, although in this case

603 female meiocytes have shorter loop-size, longer SC and more crossovers (48).

604

605 It has been reported previously that effective crossover interference is stronger in females than

606 in males in Arabidopsis (35). Our analyses indicate that the interference signal is propagated

607 over the same physical distance (μm SC) in both male and female meiosis, and thus from a
608 mechanistic standpoint interference is identical in the two sexes. The higher *effective*
609 interference (i.e. the effect on the inheritance of two linked genetic loci) observed in females
610 can be entirely explained by the difference in SC length between the two sexes, as a given
611 distance in μm SC corresponds to a greater length in Mb. It is worth noting that our estimates
612 of L_{BF} for male ($27.7 \pm 5.6 \mu\text{m}$) and female ($23.7 \pm 2.5 \mu\text{m}$) Arabidopsis are similar to estimates
613 for tomato ($14 \mu\text{m}$, ref 9) but are 80 to 90-fold larger than for yeast ($0.3 \mu\text{m}$, ref 9). This vast
614 difference in the distance across which interference propagates in different taxa, as estimated
615 by the beam-film model, remains challenging to explain biologically.

616

617 In addition to explaining differences in effective interference, SC length also explained the
618 differences in CO distribution observed between the sexes. In male meiosis, crossovers are
619 high adjacent to the peri-centromeres and in the distal regions, while in female meiosis
620 crossovers are high adjacent to the peri-centromeres but low in the distal regions (29, 39). Our
621 modelling shows that increases in the proportion of the chromosome over which interference
622 spreads (either through a reduction in SC length, or an increase in L_{BF}) reduces crossovers
623 particularly in distal regions. The lower SC length in females can therefore account for the
624 observed differences in crossover distribution.

625

626 In mammals, SC length is correlated with the number of DSBs (31, 41, 49). If the same holds
627 true in plants, then we might expect fewer DSBs in female meiosis. Our analysis revealed that
628 while the number of DSBs had very little influence on crossover distributions and CoC curves,
629 a decrease in the number of DSBs resulted in an increase in the estimated proportion of DSB
630 sites that become class II crossovers (*T2Prob*). Thus, the reduction in SC length observed for
631 females, if accompanied by an equivalent reduction in DSBs, can also account for proposed

632 differences in the number of class II crossovers between male and female meiosis. At least one
633 line of evidence suggests this question may not be fully resolved however. In mutant lines with
634 large numbers of additional class II crossovers, the recombination landscape of male and
635 female meiosis are roughly equivalent with even a slightly higher number of crossovers in
636 female (34). This suggests the possibility of similar numbers of DSBs in male and female
637 meiosis. Further comparative cytological studies of male and female meiosis will be required
638 to fully answer these questions, for example it would be interesting to see if SC lengths still
639 differ between male and female in these mutant contexts.

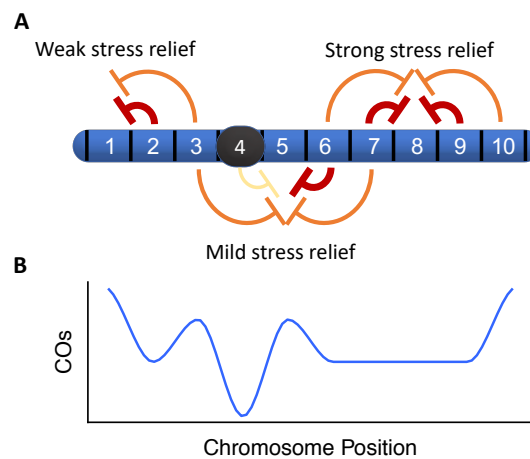
640

641 Given the substantial differences in crossover patterning between female and male meiosis it
642 is striking that they can all be accounted for by the difference in SC length. It is similarly
643 striking that despite the differences in crossover patterning there are also no significant
644 differences between the sexes in the estimated beam-film model parameters (if L is expressed
645 in μM SC, and the number of DSBs is reduced in line with the shorter SC in female). This
646 gives us good confidence in our approach, and suggests that similar investigations, in different
647 contexts (e.g. mutants, over expression lines, environmental conditions), could provide further
648 mechanistic insights into the factors governing crossover patterning in Arabidopsis.

649

650 When exploring the impact of varying the beam-film parameters it was clear that increased
651 crossover promoting stress (S_{max}) or decreased stress relief distance (L_{BF}) resulted in increased
652 crossovers particularly in terminal regions. Crossovers also increased in proximal regions but
653 only when the stress relief distance was low and so were not suppressed by the increase in
654 terminal crossovers (e.g. Figure 3A – $L = 0.4$ compared to Figure 3A – $L > 0.5$ and Figure 3D).
655 This is explained in the beam-film model, by the fact that additional crossovers will tend to
656 occur in regions that experience, on average, less stress relief. Additional crossovers in terminal

657 regions are only suppressed by prior crossovers in one direction i.e. crossovers located toward
 658 the centromere, in contrast additional crossovers in interstitial regions are suppressed by both
 659 distal and proximal crossovers (Figure 6). Similarly, the low precursor density at the
 660 centromere results in fewer crossovers and thus regions adjacent to the centromere experience
 661 less stress relief than interstitial regions (Figure 6), resulting in more crossovers. This is
 662 particularly true when the stress relief distance is low, and the local environment has greater
 663 effect (e.g. Figure 3A).
 664



665
 666
 667 **Figure 6. COs formed after the initial obligatory CO tend to accumulate in terminal and**
 668 **proximal regions. A)** Terminal regions (e.g. interval 1) experience weaker stress relief than
 669 interstitial regions (e.g. interval 8) as they are surrounded by fewer crossovers. Similarly,
 670 proximal regions (e.g. interval 5) experience less stress relief, due to the lower precursor
 671 number and therefore fewer COs in centromeric regions (interval 4). **B)** After designation of
 672 the first crossover (which will not be influenced by interference/stress relief), additional
 673 crossovers tend to accumulate in terminal and proximal regions due to their lower average
 674 levels of stress relief.
 675

676 In addition to mechanistic insights into the factors governing crossover patterning in
677 Arabidopsis, the model can be used to make predictions about how important agricultural goals
678 such as heightened recombination rates could be achieved. For example, with the development
679 of CRISPR and related technologies, it is possible to modulate the number or location of DSBs
680 in early meiosis and there is interest in using this approach to alter recombination rates in plant
681 breeding programs (50–52). In most organisms, crossover numbers are thought to be
682 maintained independently from the number of DSBs through crossover homeostasis (43–45).
683 Our modelling suggests that the extent to which homeostasis maintains crossover numbers is
684 determined by the proportion of DSBs that become class II crossovers: The higher the
685 proportion of class II crossovers, the more DSB number will affect crossover number. Thus,
686 we predict that combining the knock out of class II CO suppressing proteins (e.g. RECQ4,
687 FANCM, FIGL1, 53–55) with approaches to increase meiotic DSBs could maximize increases
688 in recombination and the associated benefit to breeding programs.

689

690 One of the surprising findings of our analysis is that for small inter-interval distances, an
691 increase in the distance over which the interference signal is propagated can result in increased
692 values of CoC (Figure 3) i.e. decreased effective interference. This behavior is not specific to
693 the beam-film model but is expected whenever both class I and class II crossovers occur, and
694 there is a change in the strength of suppression of closely spaced class I crossovers. This finding
695 highlights the need for caution when interpreting interference data and particularly in the
696 distinction between mechanistic (e.g. L_{BF}) and effective (e.g. CoC from genetic data)
697 measurements of interference. It should also be noted that at small inter-interval distances the
698 magnitude of the predicted change in CoC is small, and that for specific interval pairs the effect
699 of the local chromosomal landscape (e.g. recombination hotspots etc) may out-weigh the effect
700 predicted by the model. Despite these caveats, it is clear that an increase or decrease in

701 *mechanistic* interference strength (L_{BF}) is not expected to result in an equivalent increase or
702 decrease respectively in *effective* interference for small IIDs. Given the widespread use of
703 reporter lines that determine recombination rates and CoC values for closely linked intervals
704 (56) it is important to realize that these lines may give little to no insight into any change in the
705 mechanics of crossover interference.

706

707 As an example, two recent papers investigated altered recombination rates at temperature
708 extremes in *Arabidopsis* (57, 58). In both cases, increased temperature gave rise to more class
709 I COs, but the increased COs were associated with no change, or a decrease in genetic
710 measurements of CoC (i.e. effective interference). In the studies, CoC (or interference ratio)
711 was measured by tracking the inheritance of closely linked fluorescent reporter genes in pollen,
712 and thus combined both class I and class II crossovers measured at a small inter-interval
713 distance. While it could be concluded from these studies that temperature increases class I
714 crossovers without any effect on interference, these results are also consistent with an
715 alternative hypothesis i.e. that increased temperature decreases the distance over which
716 interference is propagated, resulting in increased class I COs, but with no effect on genetic
717 measurements of interference at small-inter-interval distances. Or to put it another way, high
718 temperature might decrease *mechanistic* interference, but result in an increase (or no change)
719 in *effective* interference for small IIDs. There is good evidence that heightened temperature
720 might have such a mechanistic effect, given that the chromosome axis is thought to mediate
721 interference (3) and the synaptonemal complex / axis structure is sensitive to temperature (59,
722 60) but this remains to be experimentally validated.

723

724 While the beam-film model was able to reliably model genetic recombination data, there are
725 several ways in which models of crossover patterning might further be improved with increased

726 understanding of the underlying biology. For example, when calculating L_{BF} and L_{CoC} in μm
727 SC using back-cross data, we assume a direct relationship between SC length and Mb. In
728 Arabidopsis the relationship between SC length and Mb is constant between whole
729 chromosomes ($R^2 = 0.99$, based on data from (61)), however the relationship may not be
730 constant within a chromosome (62). Establishing how the relationship between Mb and μm SC
731 changes for different chromosomal domains would provide one means to improve models of
732 crossover patterning when using genetic data. Another question is whether DSB density is
733 constant along the length of the chromosome? If so, is it constant relative to SC length or length
734 in Mb? Recently Spo11-oligo sequencing has demonstrated relatively constant DSB formation
735 along the length of the chromosome, although there are clearly regions of higher and lower
736 DSB density, particularly the centromeres where DSB formation is strongly suppressed (38).
737 It would be interesting to incorporate such data into future models of crossover patterning.

738

739 Despite these possible improvements to future models, it is clear that we can gain novel insights
740 into crossover patterning using genetic recombination data in combination with beam-film
741 simulations. These are particularly powerful when, as for this study, we have good estimates
742 of SC length for all chromosomes, circumventing the need for cytological determination of
743 crossover locations. This enables us to take advantage of the main benefit of genetic data, that
744 it incorporates all crossover events, and thus enables us to develop a more nuanced
745 understanding of the interplay between the mechanistic determinants of crossover-interference
746 and the final effect on patterns of inheritance.

747

748

ACKNOWLEDGEMENTS

749 We thank Christine Mezard for providing the experimental Arabidopsis recombination dataset
750 and for critical reading of the manuscript. A.L. was funded by a Marie Curie fellowship (PIOF-

751 GA-2013-628128) and the European Union's Horizon 2020 research and innovation program
752 under the Marie Skłodowska-Curie grant agreement No 663830. The IJPB benefits from the
753 support of the LabEx Saclay Plant Sciences-SPS (ANR-10-LABX-0040-SPS).

754
755
756
757
758
759
760
761
762
763
764
765
766
767
768
769
770
771
772
773
774
775
776
777
778

REFERENCES

1. Sturtevant AH (1915) The behavior of the chromosomes as studied through linkage. *Z Indukt Abstamm Vererbungsl* 13:234–287.
2. Muller HJ (1916) The Mechanism of Crossing-Over . II. *Am Nat* 50:284–305.
3. Zickler D, Kleckner N (2015) Recombination, pairing, and synapsis of homologs during meiosis. *Cold Spring Harb Perspect Biol* 7:a016626.
4. Zhang L, et al. (2014) Topoisomerase II mediates meiotic crossover interference. *Nature*:18–20.
5. Mcpeck MS, Speed TP (1995) Modeling Interference in Genetic Recombination. *Genetics* 139:1031–1044.
6. Housworth EA, Stahl FW (2003) Crossover Interference in Humans. *Genetics* 164:188–197.
7. Broman KW, Weber JL (2000) Characterization of Human Crossover Interference. *Genetics* 155:1911–1926.
8. Kleckner N, et al. (2004) A mechanical basis for chromosome function. *Proc Natl Acad Sci* 101:12592–12597.
9. Zhang L, Liang Z, Hutchinson J, Kleckner N (2014) Crossover patterning by the beam-film model: analysis and implications. *PLoS Genet* 10:e1004042.
10. Sym M, Engebrecht J, Roeder GS (1993) ZIP1 is a synaptonemal complex protein required for meiotic chromosome synapsis. *Cell* 72:365–378.
11. Chua PR, Roeder GS (1998) Zip2, a Meiosis-Specific Protein Required for the Initiation of Chromosome Synapsis. *Cell* 93:349–359.
12. Agarwal S, Roeder GS (2000) Zip3 provides a link between recombination enzymes and synaptonemal complex proteins. *Cell* 102:245–255.
13. Tsubouchi T, Zhao H, Roeder GS (2006) The Meiosis-Specific Zip4 Protein Regulates Crossover Distribution by Promoting Synaptonemal Complex Formation Together

- 779 with Zip2. *Dev Cell* 10:809–819.
- 780 14. Hollingsworth NM, Ponte L, Halsey C (1995) MSH5, a novel MutS homolog,
781 facilitates meiotic reciprocal recombination between homologs in *Saccharomyces*
782 *cerevisiae* but not mismatch repair. *Genes Dev* 9:1728–1739.
- 783 15. Ross-Macdonald P, Roeder GS (1994) Mutation of a meiosis-specific MutS homolog
784 decreases crossing over but not mismatch correction. *Cell* 79:1069–1080.
- 785 16. Nakagawa T, Ogawa H (1999) The *Saccharomyces cerevisiae* MER3 gene, encoding a
786 novel helicase-like protein, is required for crossover control in meiosis. *EMBO J*
787 18:5714–5723.
- 788 17. Lynn A, Soucek R, Börner GV (2007) ZMM proteins during meiosis : Crossover
789 artists at work. *Chromosom Res* 15:591–605.
- 790 18. Lhuissier FGP, Offenberg HH, Wittich PE, Vischer NOE, Heyting C (2007) The
791 Mismatch Repair Protein MLH1 Marks a Subset of Strongly Interfering Crossovers in
792 Tomato. *Plant Cell Online* 19:862–876.
- 793 19. Chelysheva L, et al. (2012) The Arabidopsis HEI10 is a new ZMM protein related to
794 Zip3. *PLoS Genet* 8:e1002799.
- 795 20. Hollingsworth NM, Brill SJ (2004) The Mus81 solution to resolution: Generating
796 meiotic crossovers without Holliday junctions. *Genes Dev* 18:117–125.
- 797 21. Kurzbauer M-T, et al. (2018) Arabidopsis thaliana FANCD2 Promotes Meiotic
798 Crossover Formation. *Plant Cell* 30:tpc.00745.2017.
- 799 22. Mercier R, et al. (2005) Two Meiotic Crossover Classes Cohabit in Arabidopsis : One
800 Is Dependent on MER3 , whereas the Other One Is Not. *Curr Biol* 15:692–701.
- 801 23. Cooper TJ, Crawford MR, Hunt LJ, Llorente B (2018) Mismatch repair impedes
802 meiotic crossover interference.
- 803 24. Falque M, Anderson LK, Stack SM, Gauthier F, Martin OC (2009) Two Types of

- 804 Meiotic Crossovers Coexist in Maize. *Plant Cell* 21:3915–3925.
- 805 25. White MA, Wang S, Zhang L, Kleckner N (2017) Quantitative Modeling and
806 Automated Analysis of Meiotic Recombination. *Meiosis*, ed Stuart DT (Springer New
807 York, New York, NY), pp 305–323.
- 808 26. Wang S, Zickler D, Kleckner N, Zhang L (2015) Meiotic crossover patterns:
809 Obligatory crossover, interference and homeostasis in a single process. *Cell Cycle*
810 14:305–314.
- 811 27. Loidl J (2016) Conservation and Variability of Meiosis Across the Eukaryotes. *Annu*
812 *Rev Genet* 50:293–316.
- 813 28. Mercier R, Mezard C, Jenczewski E, Macaisne N, Grelon M (2014) The Molecular
814 Biology of Meiosis in Plants. *Annu Rev Plant Biol* 66:1–31.
- 815 29. Giraut L, et al. (2011) Genome-wide crossover distribution in *Arabidopsis thaliana*
816 meiosis reveals sex-specific patterns along chromosomes. *PLoS Genet* 7:e1002354.
- 817 30. Singer A, et al. (2002) 34. Sex-Specific Recombination Rates in Zebrafish (*Danio*
818 *rerio*).pdf. 657:649–657.
- 819 31. Gruhn JR, Rubio C, Broman KW, Hunt PA, Hassold T (2013) Cytological studies of
820 human meiosis: Sex-specific differences in recombination originate at, or prior to,
821 establishment of double-strand breaks. *PLoS One* 8:1–15.
- 822 32. Tortereau F, et al. (2012) A high density recombination map of the pig reveals a
823 correlation between sex-specific recombination and GC content. *BMC Genomics* 13.
824 doi:10.1186/1471-2164-13-586.
- 825 33. Phillips D, et al. (2015) The effect of temperature on the male and female
826 recombination landscape of barley. *New Phytol* 208:421–429.
- 827 34. Fernandes JB, Seguéla-Arnaud M, Larchevêque C, Lloyd AH, Mercier R (2017)
828 Unleashing meiotic crossovers in hybrid plants. *Proc Natl Acad Sci*:201713078.

- 829 35. Basu-roy S, Gauthier F, Giraut L, Mézard C (2013) Hot Regions of Noninterfering
830 Crossovers Coexist with a Nonuniformly Interfering Pathway in. *Genetics* 195:769–
831 779.
- 832 36. White MA, Wang S, Zhang L, Kleckner N (2017) Quantitative Modeling and
833 Automated Analysis of Meiotic Recombination. *Methods Mol Biol* 1471:305–323.
- 834 37. Berchowitz LE, Copenhaver GP (2010) Genetic interference: don't stand so close to
835 me. *Curr Genomics* 11:91–102.
- 836 38. Choi K, et al. (2018) Nucleosomes and DNA methylation shape meiotic DSB
837 frequency in *Arabidopsis thaliana* transposons and gene regulatory regions. *Genome*
838 *Res* 28:1–15.
- 839 39. Drouaud J, et al. (2007) Sex-specific crossover distributions and variations in
840 interference level along *Arabidopsis thaliana* chromosome 4. *PLoS Genet* 3:e106.
- 841 40. Panizza S, et al. (2011) Spo11-accessory proteins link double-strand break sites to the
842 chromosome axis in early meiotic recombination. *Cell* 146:372–83.
- 843 41. Baier B, Hunt P, Broman KW, Hassold T (2014) Variation in Genome-Wide Levels of
844 Meiotic Recombination Is Established at the Onset of Prophase in Mammalian Males.
845 *PLoS Genet* 10. doi:10.1371/journal.pgen.1004125.
- 846 42. Anderson LK, et al. (2014) Combined fluorescent and electron microscopic imaging
847 unveils the specific properties of two classes of meiotic crossovers. *Proc Natl Acad Sci*
848 *USA* 111:13415–13420.
- 849 43. Cole F, et al. (2012) Homeostatic control of recombination is implemented
850 progressively in mouse meiosis. *Nat Cell Biol* 14:424.
- 851 44. Martini E, Diaz RL, Hunter N, Keeney S (2006) Crossover Homeostasis in Yeast
852 Meiosis. *Cell* 126:285–295.
- 853 45. Rosu S, Libuda DE, Villeneuve AM (2011) Robust crossover assurance and regulated

- 854 interhomolog access maintain meiotic crossover number. *Science* 334:1286–9.
- 855 46. Zickler D, Kleckner N (1999) Integrating Structure and Function. *Annu Rev Genet*
856 33:603–754.
- 857 47. Kaiser VB, Semple CA (2018) Chromatin loop anchors are associated with genome
858 instability in cancer and recombination hotspots in the germline. *Genome Biol* 19:1–
859 14.
- 860 48. Tease C, Hultén MA (2004) Inter-sex variation in synaptonemal complex lengths
861 largely determine the different recombination rates in male and female germ cells.
862 *Cytogenet Genome Res* 107:208–215.
- 863 49. Ruiz-Herrera A, et al. (2017) Recombination correlates with synaptonemal complex
864 length and chromatin loop size in bovids—insights into mammalian meiotic
865 chromosomal organization. *Chromosoma* 126:615–631.
- 866 50. Puchta H (2017) Applying CRISPR/Cas for genome engineering in plants: the best is
867 yet to come. *Curr Opin Plant Biol* 36:1–8.
- 868 51. Hayut SF, Bessudo CM, Levy AA (2017) Targeted recombination between
869 homologous chromosomes for precise breeding in tomato. *Nat Commun* 8:1–9.
- 870 52. Choi K (2017) Advances towards Controlling Meiotic Recombination for Plant
871 Breeding. *Mol Cells* 40:814–822.
- 872 53. Crismani W, et al. (2012) FANCM Limits Meiotic Crossovers. *Science* 336:1588–
873 1590.
- 874 54. Seguela-Arnaud M, et al. (2015) Multiple mechanisms limit meiotic crossovers : TOP3
875 α and two BLM homologs antagonize crossovers in parallel to FANCM. 112.
876 doi:10.1073/pnas.1423107112.
- 877 55. Girard C, et al. (2015) AAA-ATPase FIDGETIN-LIKE 1 and Helicase FANCM
878 Antagonize Meiotic Crossovers by Distinct Mechanisms. *PLOS Genet* 11:e1005369.

- 879 56. Francis KE, et al. (2007) Pollen tetrad-based visual assay for meiotic recombination in
880 *Arabidopsis*. *Proc Natl Acad Sci U S A* 104:3913–8.
- 881 57. Lloyd A, Morgan C, Franklin C, Bomblies K (2018) Plasticity of meiotic
882 recombination rates in response to temperature in *Arabidopsis*.
- 883 58. Modliszewski JL, et al. (2018) Elevated temperature increases meiotic crossover
884 frequency via the interfering (Type I) pathway in *Arabidopsis thaliana*. *PLoS Genet*
885 14:1–15.
- 886 59. Loidl J (1989) Effects of elevated temperature on meiotic chromosome synapsis in
887 *Allium ursinum*. *Chromosoma* 97:449–458.
- 888 60. Morgan CH, Zhang H, Bomblies K (2017) Are the effects of elevated temperature on
889 meiotic recombination and thermotolerance linked via the axis and synaptonemal
890 complex? *Philos Trans R Soc B Biol Sci* 372. doi:10.1098/rstb.2016.0470.
- 891 61. López E, Pradillo M, Romero C, Santos JL, Cuñado N (2008) Pairing and synapsis in
892 wild type *Arabidopsis thaliana*. *Chromosom Res* 16:701–708.
- 893 62. Bickmore WA, Oghene K (1996) Visualizing the spatial relationships between defined
894 DNA sequences and the axial region of extracted metaphase chromosomes. *Cell*
895 84:95–104.
- 896

897 **Figure 1. Crossover analysis for Arabidopsis chromosome 5.** Each analysis includes
898 experimental (solid lines) and simulated (dashed lines) data for male (blue) and female
899 (orange). **A** Crossover distributions for Arabidopsis chromosome 5. Dashed lines represent the
900 limits of the centromeric region over which precursor (DSB) number is markedly reduced both
901 biologically (38) and during simulations. Error bars indicate 95% confidence intervals. **B-C**
902 CoC curves for chromosome 5 with inter-interval distance (IID, the distance between a pair of
903 genetic intervals) measured in Mb (**B**) or μm SC (**C**). L_{CoC} for male and female (blue and orange
904 arrows respectively) differed when IIDs were measured in Mb but not when measured in μm
905 SC. **D** Event distribution for chromosome 5. Male and female simulations shown, assume 250
906 DSBs genome-wide. Chromosomes were divided into 13 equal-sized adjacent intervals for
907 analysis.
908

909 **Figure 2. Beam-film best-fit parameter estimates.** **A)** Estimates of crossover promoting
910 force (S_{max}) were identical for male and female with 250 DSBs (M and F respectively), and
911 female with 150 DSBs (F_{DSB}). Estimates of interference distance (L) were longer in male when
912 measured in Mb (**B**) but not significantly different when measured in μm SC (**C**). **D)** There
913 was no significant difference in estimates of chromosome clamping. **E)** The probability of non-
914 class I-designated precursors becoming class II crossovers was estimated to be lower in female
915 than male if both sexes had 250 DSBs, but not significantly different if there are reduced DSBs
916 (150) in female. For each parameter and condition, the mean of the estimates for the five
917 chromosomes is shown. Error bars indicate 95% confidence interval. * $p < 0.05$, ** $p < 0.01$,
918 after Bonferroni multiple comparison correction.
919

920 **Figure 3. Effect of beam-film parameters on crossover patterning in Arabidopsis.** The
921 effect of altering a single beam film parameter – L (**A-C**), Smax (**D-F**) or T2Prob (**G-I**) – on
922 crossover distribution (**A, D & G**) and CoC (**B-C, E-F** and **H-I**). Red vertical lines in **C, F** and
923 **I** represent IID = 0.1. Grey shading in CoC curves indicate 95% confidence interval.
924

925 **Figure 4. Influence of IID on CoC response to changes in L_{BF} .** **A** The expected (solid line)
926 and observed (dashed line) proportion of interval pairs receiving a double crossover (DCO) for
927 two different inter-interval distances (IIDs); calculated from simulations with varying values
928 of L_{BF} . **B** CoC values for two IIDs calculated from simulations with varying values of L_{BF} . **C**
929 The number of DCOs observed for different IIDs from simulations involving class I and class
930 II crossovers (CI & CII), class I crossovers only (CI) or class II crossovers only (CII). **D** The
931 proportions of DCOs formed between two class I crossovers (CI_CI), two class II crossovers
932 (CII_CII), or a class I and a class II CO (CI_CII) for different IIDs.
933

934 **Figure 5. Influence of DSB number on crossover patterning and homeostasis is**
935 **dependent on the probability of class II crossovers.** A-C show results for simulations of
936 wild type meiosis, D-F show results for simulation of meiosis with increased class II crossover
937 formation (T2Prob). **A)** Increased DSBs in wild type resulted in more proximal and distal
938 crossovers, but fewer interstitial crossovers. **D)** In mutants with increased class II crossovers,
939 more DSBs resulted in a uniform increase in crossovers. **B-C)** For wild type, CoC values
940 increased at small inter-interval distances with increased DSBs. **E-F)** With increased class II
941 COs, CoC values were ~1 for all inter-interval distances and all DSB numbers. **(G)** Total
942 crossover number for genome-wide simulations using best-fit parameters for male and female
943 meiosis and varying numbers of DSBs. In wild type (dashed lines) increasing DSBs had a
944 minimal effect on total crossovers. With increased class II COs (solid lines) doubling DSBs
945 resulted in twice as many crossovers. Grey shading in CoC curves indicates 95% confidence
946 interval.
947

948 **Figure 6. Crossover increases tend to accumulate in terminal and proximal regions. A)**
949 Terminal regions (e.g. interval 1) experience weaker stress relief than interstitial regions (e.g.
950 interval 8) as they are surrounded by fewer crossovers. Similarly, proximal regions (e.g.
951 interval 5) experience less stress relief, due to the lower precursor number and therefore fewer
952 COs in centromeric regions (interval 4). **B)** As crossovers increase, the additional crossovers
953 tend to accumulate in terminal and proximal regions due to their lower average levels of stress
954 relief.
955

956 **Table 1. L_{CoC} values**

	Mb			$\mu\text{m SC}$		
	male	female	p value [#]	male	female	p value [#]
experimental	7.05 ± 0.50	12.84 ± 1.50	7.90E-07	11.65 ± 0.86	12.83 ± 1.50	1
simulated	6.30 ± 1.05	11.60 ± 0.83	1.40E-05	10.21 ± 1.75	11.20 ± 0.78	1
p value [#]	1	1		1	1	

[#]Bonferroni multiple-comparison corrected

957

959 Table S1. Chromosome metrics and beam-film parameters

Chr	Sex	Mb	μ m SC	Beam-film parameters															
				N#	B#	E#	Bs#	Be#	Bd#	Smax [^]	Bsmax#	A#	Lp [^]	Lmb*	Lsc*	cL [^]	cR [^]	M#	T2prob [^]
1	M	30.4	49.2	64	1	0.6	0.475	0.5	0.01	8.5	1	1	0.65	19.8	32.0	0.8	1	1	0.005
2	M	19.7	31.9	41	1	0.6	0.175	0.225	0.01	7.5	1	1	0.85	16.7	27.1	0.3	0.9	1	0.0065
3	M	23.5	37.9	49	1	0.6	0.5	0.65	0.01	5.5	1	1	0.7	16.4	26.6	0.4	0.9	1	0.008
4	M	18.6	30.1	39	1	0.6	0.125	0.225	0.01	4	1	1	0.6	11.2	18.0	0.6	0.9	1	0.0055
5	M	27.0	43.6	56	1	0.6	0.4	0.5	0.01	9.5	1	1	0.8	21.6	34.9	1.1	0.9	1	0.0065
1	F	30.4	25.0	64	1	0.6	0.475	0.5	0.01	8	1	1	1	30.4	25.0	0.7	0.5	1	0.003
2	F	19.7	16.2	41	1	0.6	0.175	0.25	0.01	7	1	1	1.6	31.5	25.9	1.2	0.8	1	0.004
3	F	23.5	19.3	49	1	0.6	0.5	0.65	0.01	6	1	1	1	23.5	19.3	0.5	0.6	1	0.005
4	F	18.6	15.3	39	1	0.6	0.125	0.225	0.01	7	1	1	1.7	31.6	26.0	0.8	0.5	1	0.003
5	F	27.0	22.2	56	1	0.6	0.4	0.5	0.01	6.5	1	1	1	27.0	22.2	0.7	0.6	1	0.003
1	F _{DSB}	30.4	25.0	38	1	0.6	0.475	0.525	0.01	7	1	1	0.9	27.4	22.5	0.5	0.7	1	0.006
2	F _{DSB}	19.7	16.2	38	1	0.6	0.475	0.525	0.01	6.5	1	1	1.5	29.6	24.3	1	0.8	1	0.004
3	F _{DSB}	23.5	19.3	29	1	0.6	0.5	0.65	0.01	6	1	1	1	23.5	19.3	0.5	0.6	1	0.008
4	F _{DSB}	18.6	15.3	23	1	0.6	0.125	0.225	0.01	6	1	1	1.7	31.6	26.0	0.8	0.4	1	0.005
5	F _{DSB}	27.0	22.2	34	1	0.6	0.4	0.5	0.01	8.5	1	1	1.1	29.7	24.4	0.6	0.5	1	0.005

960 #Optimised parameter

961 [^]Fixed parameter962 *Calculated based on L_p

963

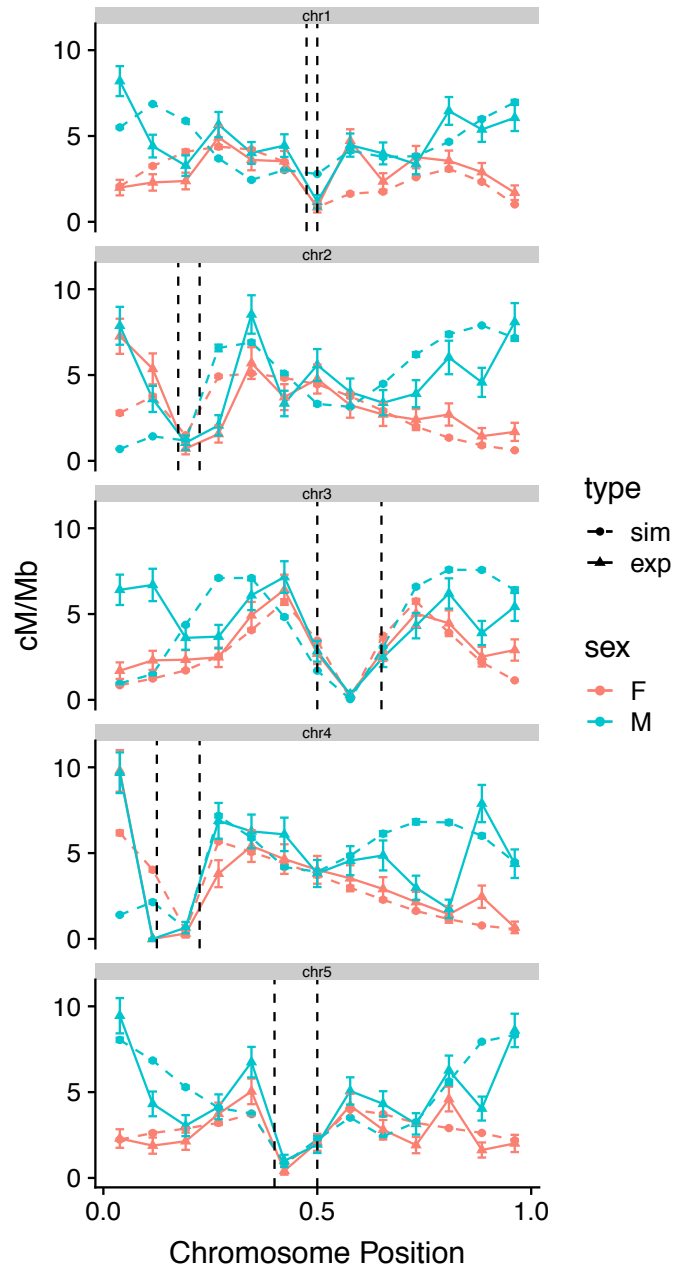
Table S2. Beam-film parameters used for simulations shown in each figure.

Figure	Part	Details	Beam-film parameters													
			N	B	E	Bs	Be	Bd	Smax	Bsmax	A	L	cL	cR	M	T2prob
1	A-D	male	56	1	0.6	0.4	0.5	0.01	9.5	1	1	0.8	1.1	0.9	1	0.0065
1	A-D	female	56	1	0.6	0.4	0.5	0.01	6.5	1	1	1	0.7	0.6	1	0.003
3	A-C	L - 0.4	60	1	0.6	0.45	0.55	0.01	7	1	1	0.4	0.8	0.8	1	0.004
3	A-C	L - 0.7	60	1	0.6	0.45	0.55	0.01	7	1	1	0.7	0.8	0.8	1	0.004
3	A-C	L - 1	60	1	0.6	0.45	0.55	0.01	7	1	1	1	0.8	0.8	1	0.004
3	A-C	L - 1.3	60	1	0.6	0.45	0.55	0.01	7	1	1	1.3	0.8	0.8	1	0.004
3	D-F	Smax - 3	60	1	0.6	0.45	0.55	0.01	3	1	1	0.7	0.8	0.8	1	0.004
3	D-F	Smax - 5	60	1	0.6	0.45	0.55	0.01	5	1	1	0.7	0.8	0.8	1	0.004
3	D-F	Smax - 7	60	1	0.6	0.45	0.55	0.01	7	1	1	0.7	0.8	0.8	1	0.004
3	D-F	Smax - 9	60	1	0.6	0.45	0.55	0.01	9	1	1	0.7	0.8	0.8	1	0.004
3	G-I	T2prob - 0	60	1	0.6	0.45	0.55	0.01	9	1	1	0.7	0.8	0.8	1	0
3	G-I	T2prob - 0.002	60	1	0.6	0.45	0.55	0.01	9	1	1	0.7	0.8	0.8	1	0.002
3	G-I	T2prob - 0.004	60	1	0.6	0.45	0.55	0.01	9	1	1	0.7	0.8	0.8	1	0.004
3	G-I	T2prob - 0.006	60	1	0.6	0.45	0.55	0.01	9	1	1	0.7	0.8	0.8	1	0.006
4	A-B	L - 0.8	60	1	0.6	0.45	0.55	0.01	7	1	1	0.8	0.8	0.8	1	0.004
4	A-B	L - 0.9	60	1	0.6	0.45	0.55	0.01	7	1	1	0.9	0.8	0.8	1	0.004
4	A-B	L - 1	60	1	0.6	0.45	0.55	0.01	7	1	1	1	0.8	0.8	1	0.004
4	A-B	L - 1.1	60	1	0.6	0.45	0.55	0.01	7	1	1	1.1	0.8	0.8	1	0.004
4	C-D	CI	60	1	0.6	0.45	0.55	0.01	7	1	1	0.7	0.8	0.8	1	0
4	C-D	CII	60	1	0.6	0.45	0.55	0.01	0	1	1	0.7	0.8	0.8	1	0.004
4	C-D	CI & CII	60	1	0.6	0.45	0.55	0.01	7	1	1	0.7	0.8	0.8	1	0.004
5	A-C	wt	30	1	0.6	0.45	0.55	0.01	9	1	1	0.7	0.8	0.8	1	0.004
5	A-C	wt	60	1	0.6	0.45	0.55	0.01	9	1	1	0.7	0.8	0.8	1	0.004
5	A-C	wt	90	1	0.6	0.45	0.55	0.01	9	1	1	0.7	0.8	0.8	1	0.004
5	A-C	wt	120	1	0.6	0.45	0.55	0.01	9	1	1	0.7	0.8	0.8	1	0.004
5	D-F	mut	30	1	0.6	0.45	0.55	0.01	9	1	1	0.7	0.8	0.8	1	0.2
5	D-F	mut	60	1	0.6	0.45	0.55	0.01	9	1	1	0.7	0.8	0.8	1	0.2
5	D-F	mut	90	1	0.6	0.45	0.55	0.01	9	1	1	0.7	0.8	0.8	1	0.2
5	D-F	mut	120	1	0.6	0.45	0.55	0.01	9	1	1	0.7	0.8	0.8	1	0.2
5	G	wt male - chr 1 - 125 DSBs	32	1	0.6	0.48	0.5	0.01	8.5	1	1	0.65	0.8	1	1	0.005
5	G	wt male - chr 2 - 125 DSBs	21	1	0.6	0.18	0.23	0.01	7.5	1	1	0.85	0.3	0.9	1	0.0065
5	G	wt male - chr 3 - 125 DSBs	25	1	0.6	0.5	0.65	0.01	5.5	1	1	0.7	0.4	0.9	1	0.008
5	G	wt male - chr 4 - 125 DSBs	19	1	0.6	0.13	0.23	0.01	4	1	1	0.6	0.6	0.9	1	0.0055
5	G	wt male - chr 5 - 125 DSBs	28	1	0.6	0.4	0.5	0.01	9.5	1	1	0.8	1.1	0.9	1	0.0065
5	G	wt male - chr 1 - 250 DSBs	64	1	0.6	0.48	0.5	0.01	8.5	1	1	0.65	0.8	1	1	0.005
5	G	wt male - chr 2 - 250 DSBs	42	1	0.6	0.18	0.23	0.01	7.5	1	1	0.85	0.3	0.9	1	0.0065
5	G	wt male - chr 3 - 250 DSBs	49	1	0.6	0.5	0.65	0.01	5.5	1	1	0.7	0.4	0.9	1	0.008
5	G	wt male - chr 4 - 250 DSBs	39	1	0.6	0.13	0.23	0.01	4	1	1	0.6	0.6	0.9	1	0.0055
5	G	wt male - chr 5 - 250 DSBs	56	1	0.6	0.4	0.5	0.01	9.5	1	1	0.8	1.1	0.9	1	0.0065
5	G	wt male - chr 1 - 375 DSBs	96	1	0.6	0.48	0.5	0.01	8.5	1	1	0.65	0.8	1	1	0.005
5	G	wt male - chr 2 - 375 DSBs	63	1	0.6	0.18	0.23	0.01	7.5	1	1	0.85	0.3	0.9	1	0.0065
5	G	wt male - chr 3 - 375 DSBs	75	1	0.6	0.5	0.65	0.01	5.5	1	1	0.7	0.4	0.9	1	0.008
5	G	wt male - chr 4 - 375 DSBs	57	1	0.6	0.13	0.23	0.01	4	1	1	0.6	0.6	0.9	1	0.0055
5	G	wt male - chr 5 - 375 DSBs	84	1	0.6	0.4	0.5	0.01	9.5	1	1	0.8	1.1	0.9	1	0.0065
5	G	wt male - chr 1 - 500 DSBs	128	1	0.6	0.48	0.5	0.01	8.5	1	1	0.65	0.8	1	1	0.005
5	G	wt male - chr 2 - 500 DSBs	84	1	0.6	0.18	0.23	0.01	7.5	1	1	0.85	0.3	0.9	1	0.0065
5	G	wt male - chr 3 - 500 DSBs	98	1	0.6	0.5	0.65	0.01	5.5	1	1	0.7	0.4	0.9	1	0.008
5	G	wt male - chr 4 - 500 DSBs	78	1	0.6	0.13	0.23	0.01	4	1	1	0.6	0.6	0.9	1	0.0055
5	G	wt male - chr 5 - 500 DSBs	112	1	0.6	0.4	0.5	0.01	9.5	1	1	0.8	1.1	0.9	1	0.0065
5	G	mut male - chr 1 - 125 DSBs	32	1	0.6	0.48	0.5	0.01	8.5	1	1	0.65	0.8	1	1	0.2

5	G	mut male - chr 2 - 125 DSBs	21	1	0.6	0.18	0.23	0.01	7.5	1	1	0.85	0.3	0.9	1	0.2
5	G	mut male - chr 3 - 125 DSBs	25	1	0.6	0.5	0.65	0.01	5.5	1	1	0.7	0.4	0.9	1	0.2
5	G	mut male - chr 4 - 125 DSBs	19	1	0.6	0.13	0.23	0.01	4	1	1	0.6	0.6	0.9	1	0.2
5	G	mut male - chr 5 - 125 DSBs	28	1	0.6	0.4	0.5	0.01	9.5	1	1	0.8	1.1	0.9	1	0.2
5	G	mut male - chr 1 - 250 DSBs	64	1	0.6	0.48	0.5	0.01	8.5	1	1	0.65	0.8	1	1	0.2
5	G	mut male - chr 2 - 250 DSBs	42	1	0.6	0.18	0.23	0.01	7.5	1	1	0.85	0.3	0.9	1	0.2
5	G	mut male - chr 3 - 250 DSBs	49	1	0.6	0.5	0.65	0.01	5.5	1	1	0.7	0.4	0.9	1	0.2
5	G	mut male - chr 4 - 250 DSBs	39	1	0.6	0.13	0.23	0.01	4	1	1	0.6	0.6	0.9	1	0.2
5	G	mut male - chr 5 - 250 DSBs	56	1	0.6	0.4	0.5	0.01	9.5	1	1	0.8	1.1	0.9	1	0.2
5	G	mut male - chr 1 - 375 DSBs	96	1	0.6	0.48	0.5	0.01	8.5	1	1	0.65	0.8	1	1	0.2
5	G	mut male - chr 2 - 375 DSBs	63	1	0.6	0.18	0.23	0.01	7.5	1	1	0.85	0.3	0.9	1	0.2
5	G	mut male - chr 3 - 375 DSBs	75	1	0.6	0.5	0.65	0.01	5.5	1	1	0.7	0.4	0.9	1	0.2
5	G	mut male - chr 4 - 375 DSBs	57	1	0.6	0.13	0.23	0.01	4	1	1	0.6	0.6	0.9	1	0.2
5	G	mut male - chr 5 - 375 DSBs	84	1	0.6	0.4	0.5	0.01	9.5	1	1	0.8	1.1	0.9	1	0.2
5	G	mut male - chr 1 - 500 DSBs	128	1	0.6	0.48	0.5	0.01	8.5	1	1	0.65	0.8	1	1	0.2
5	G	mut male - chr 2 - 500 DSBs	84	1	0.6	0.18	0.23	0.01	7.5	1	1	0.85	0.3	0.9	1	0.2
5	G	mut male - chr 3 - 500 DSBs	98	1	0.6	0.5	0.65	0.01	5.5	1	1	0.7	0.4	0.9	1	0.2
5	G	mut male - chr 4 - 500 DSBs	78	1	0.6	0.13	0.23	0.01	4	1	1	0.6	0.6	0.9	1	0.2
5	G	mut male - chr 5 - 500 DSBs	112	1	0.6	0.4	0.5	0.01	9.5	1	1	0.8	1.1	0.9	1	0.2
5	G	DSBs wt female - chr 1 - 125	32	1	0.6	0.48	0.5	0.01	8	1	1	1	0.7	0.5	1	0.003
5	G	DSBs wt female - chr 2 - 125	21	1	0.6	0.18	0.25	0.01	7	1	1	1.6	1.2	0.8	1	0.004
5	G	DSBs wt female - chr 3 - 125	25	1	0.6	0.5	0.65	0.01	6	1	1	1	0.5	0.6	1	0.005
5	G	DSBs wt female - chr 4 - 125	19	1	0.6	0.13	0.23	0.01	7	1	1	1.7	0.8	0.5	1	0.003
5	G	DSBs wt female - chr 5 - 125	28	1	0.6	0.4	0.5	0.01	6.5	1	1	1	0.7	0.6	1	0.003
5	G	DSBs wt female - chr 1 - 250	64	1	0.6	0.48	0.5	0.01	8	1	1	1	0.7	0.5	1	0.003
5	G	DSBs wt female - chr 2 - 250	42	1	0.6	0.18	0.25	0.01	7	1	1	1.6	1.2	0.8	1	0.004
5	G	DSBs wt female - chr 3 - 250	49	1	0.6	0.5	0.65	0.01	6	1	1	1	0.5	0.6	1	0.005
5	G	DSBs wt female - chr 4 - 250	39	1	0.6	0.13	0.23	0.01	7	1	1	1.7	0.8	0.5	1	0.003
5	G	DSBs wt female - chr 5 - 250	56	1	0.6	0.4	0.5	0.01	6.5	1	1	1	0.7	0.6	1	0.003
5	G	DSBs wt female - chr 1 - 375	96	1	0.6	0.48	0.5	0.01	8	1	1	1	0.7	0.5	1	0.003
5	G	DSBs wt female - chr 2 - 375	63	1	0.6	0.18	0.25	0.01	7	1	1	1.6	1.2	0.8	1	0.004
5	G	DSBs wt female - chr 3 - 375	75	1	0.6	0.5	0.65	0.01	6	1	1	1	0.5	0.6	1	0.005
5	G	DSBs wt female - chr 4 - 375	57	1	0.6	0.13	0.23	0.01	7	1	1	1.7	0.8	0.5	1	0.003
5	G	DSBs wt female - chr 5 - 375	84	1	0.6	0.4	0.5	0.01	6.5	1	1	1	0.7	0.6	1	0.003
5	G	DSBs wt female - chr 1 - 500	128	1	0.6	0.48	0.5	0.01	8	1	1	1	0.7	0.5	1	0.003
5	G	DSBs wt female - chr 2 - 500	84	1	0.6	0.18	0.25	0.01	7	1	1	1.6	1.2	0.8	1	0.004
5	G	DSBs wt female - chr 3 - 500	98	1	0.6	0.5	0.65	0.01	6	1	1	1	0.5	0.6	1	0.005
5	G	DSBs wt female - chr 4 - 500	78	1	0.6	0.13	0.23	0.01	7	1	1	1.7	0.8	0.5	1	0.003
5	G	DSBs wt female - chr 5 - 500	112	1	0.6	0.4	0.5	0.01	6.5	1	1	1	0.7	0.6	1	0.003
5	G	DSBs mut female - chr 1 - 125	32	1	0.6	0.48	0.5	0.01	8	1	1	1	0.7	0.5	1	0.2
5	G	DSBs mut female - chr 2 - 125	21	1	0.6	0.18	0.25	0.01	7	1	1	1.6	1.2	0.8	1	0.2
5	G	DSBs mut female - chr 3 - 125	25	1	0.6	0.5	0.65	0.01	6	1	1	1	0.5	0.6	1	0.2
5	G	DSBs	25	1	0.6	0.5	0.65	0.01	6	1	1	1	0.5	0.6	1	0.2

5	G	mut female - chr 4 - 125 DSBs	19	1	0.6	0.13	0.23	0.01	7	1	1	1.7	0.8	0.5	1	0.2
5	G	mut female - chr 5 - 125 DSBs	28	1	0.6	0.4	0.5	0.01	6.5	1	1	1	0.7	0.6	1	0.2
5	G	mut female - chr 1 - 250 DSBs	64	1	0.6	0.48	0.5	0.01	8	1	1	1	0.7	0.5	1	0.2
5	G	mut female - chr 2 - 250 DSBs	42	1	0.6	0.18	0.25	0.01	7	1	1	1.6	1.2	0.8	1	0.2
5	G	mut female - chr 3 - 250 DSBs	49	1	0.6	0.5	0.65	0.01	6	1	1	1	0.5	0.6	1	0.2
5	G	mut female - chr 4 - 250 DSBs	39	1	0.6	0.13	0.23	0.01	7	1	1	1.7	0.8	0.5	1	0.2
5	G	mut female - chr 5 - 250 DSBs	56	1	0.6	0.4	0.5	0.01	6.5	1	1	1	0.7	0.6	1	0.2
5	G	mut female - chr 1 - 375 DSBs	96	1	0.6	0.48	0.5	0.01	8	1	1	1	0.7	0.5	1	0.2
5	G	mut female - chr 2 - 375 DSBs	63	1	0.6	0.18	0.25	0.01	7	1	1	1.6	1.2	0.8	1	0.2
5	G	mut female - chr 3 - 375 DSBs	75	1	0.6	0.5	0.65	0.01	6	1	1	1	0.5	0.6	1	0.2
5	G	mut female - chr 4 - 375 DSBs	57	1	0.6	0.13	0.23	0.01	7	1	1	1.7	0.8	0.5	1	0.2
5	G	mut female - chr 5 - 375 DSBs	84	1	0.6	0.4	0.5	0.01	6.5	1	1	1	0.7	0.6	1	0.2
5	G	mut female - chr 1 - 500 DSBs	128	1	0.6	0.48	0.5	0.01	8	1	1	1	0.7	0.5	1	0.2
5	G	mut female - chr 2 - 500 DSBs	84	1	0.6	0.18	0.25	0.01	7	1	1	1.6	1.2	0.8	1	0.2
5	G	mut female - chr 3 - 500 DSBs	98	1	0.6	0.5	0.65	0.01	6	1	1	1	0.5	0.6	1	0.2
5	G	mut female - chr 4 - 500 DSBs	78	1	0.6	0.13	0.23	0.01	7	1	1	1.7	0.8	0.5	1	0.2
5	G	mut female - chr 5 - 500 DSBs	112	1	0.6	0.4	0.5	0.01	6.5	1	1	1	0.7	0.6	1	0.2
S1 & S2	chr1	male	64	1	0.6	0.48	0.5	0.01	8.5	1	1	0.65	0.8	1	1	0.005
S1 & S2	chr1	female	64	1	0.6	0.48	0.5	0.01	8	1	1	1	0.7	0.5	1	0.003
S1 & S2	chr2	male	41	1	0.6	0.18	0.23	0.01	7.5	1	1	0.85	0.3	0.9	1	0.0065
S1 & S2	chr2	female	41	1	0.6	0.18	0.25	0.01	7	1	1	1.6	1.2	0.8	1	0.004
S1 & S2	chr3	male	49	1	0.6	0.5	0.65	0.01	5.5	1	1	0.7	0.4	0.9	1	0.008
S1 & S2	chr3	female	49	1	0.6	0.5	0.65	0.01	6	1	1	1	0.5	0.6	1	0.005
S1 & S2	chr4	male	39	1	0.6	0.13	0.23	0.01	4	1	1	0.6	0.6	0.9	1	0.0055
S1 & S2	chr4	female	39	1	0.6	0.13	0.23	0.01	7	1	1	1.7	0.8	0.5	1	0.003
S1 & S2	chr5	male	56	1	0.6	0.4	0.5	0.01	9.5	1	1	0.8	1.1	0.9	1	0.0065
S1 & S2	chr5	female	56	1	0.6	0.4	0.5	0.01	6.5	1	1	1	0.7	0.6	1	0.003
S3	chr5	low	56	1	0.6	0.4	0.5	0.01	3	1	1	1.7	0.1	0.1	1	0.002
S3	chr5	high	56	1	0.6	0.4	0.5	0.01	10	1	1	0.4	1.3	1.3	1	0.006
S4		CI - all	60	1	0.6	0.45	0.55	0.01	7	1	1	0.7	0.8	0.8	1	0
S4		CII - T2Prob 0.001	60	1	0.6	0.45	0.55	0.01	0	1	1	0.7	0.8	0.8	1	0.001
S4		CI & CII - T2Prob 0.001	60	1	0.6	0.45	0.55	0.01	7	1	1	0.7	0.8	0.8	1	0.001
S4		CII - T2Prob 0.005	60	1	0.6	0.45	0.55	0.01	0	1	1	0.7	0.8	0.8	1	0.005
S4		CI & CII - T2Prob 0.005	60	1	0.6	0.45	0.55	0.01	7	1	1	0.7	0.8	0.8	1	0.005
S4		CII - T2Prob 0.01	60	1	0.6	0.45	0.55	0.01	0	1	1	0.7	0.8	0.8	1	0.01
S4		CI & CII - T2Prob 0.01	60	1	0.6	0.45	0.55	0.01	7	1	1	0.7	0.8	0.8	1	0.01
S4		CII - T2Prob 0.025	60	1	0.6	0.45	0.55	0.01	0	1	1	0.7	0.8	0.8	1	0.025
S4		CI & CII - T2Prob 0.025	60	1	0.6	0.45	0.55	0.01	7	1	1	0.7	0.8	0.8	1	0.025

S4	CII - T2Prob 0.125	60	1	0.6	0.45	0.55	0.01	0	1	1	0.7	0.8	0.8	1	0.125
S4	CI & CII - T2Prob 0.125	60	1	0.6	0.45	0.55	0.01	7	1	1	0.7	0.8	0.8	1	0.125



966

967

968 **Figure S1. Experimental and simulated crossover distributions.** Each analysis includes

969 experimental (solid lines) and simulated (dashed lines) data for male (blue) and female (orange). Dashed

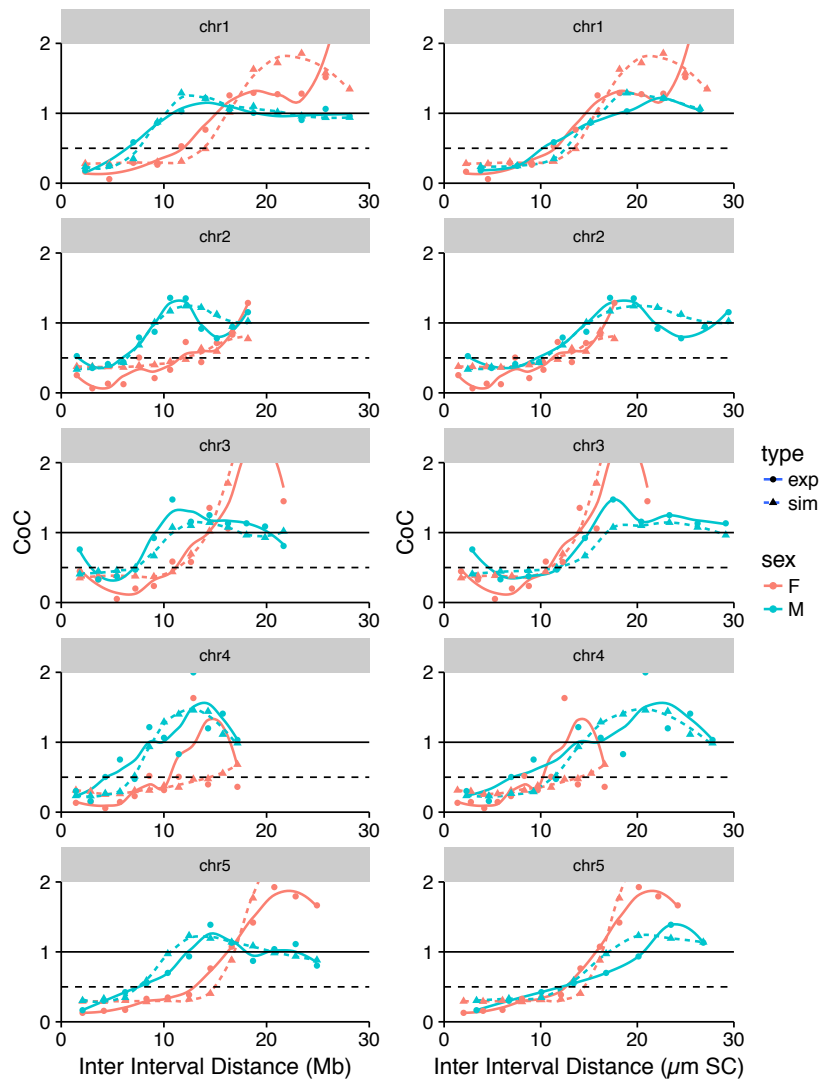
970 lines represent the limits of the centromeric region over which precursor (DSB) number is markedly

971 reduced both biologically (38) and during simulations. Male and female simulations shown, assume

972 250 DSBs genome-wide. Chromosomes were divided into 13 equal-sized adjacent intervals for

973 analysis.

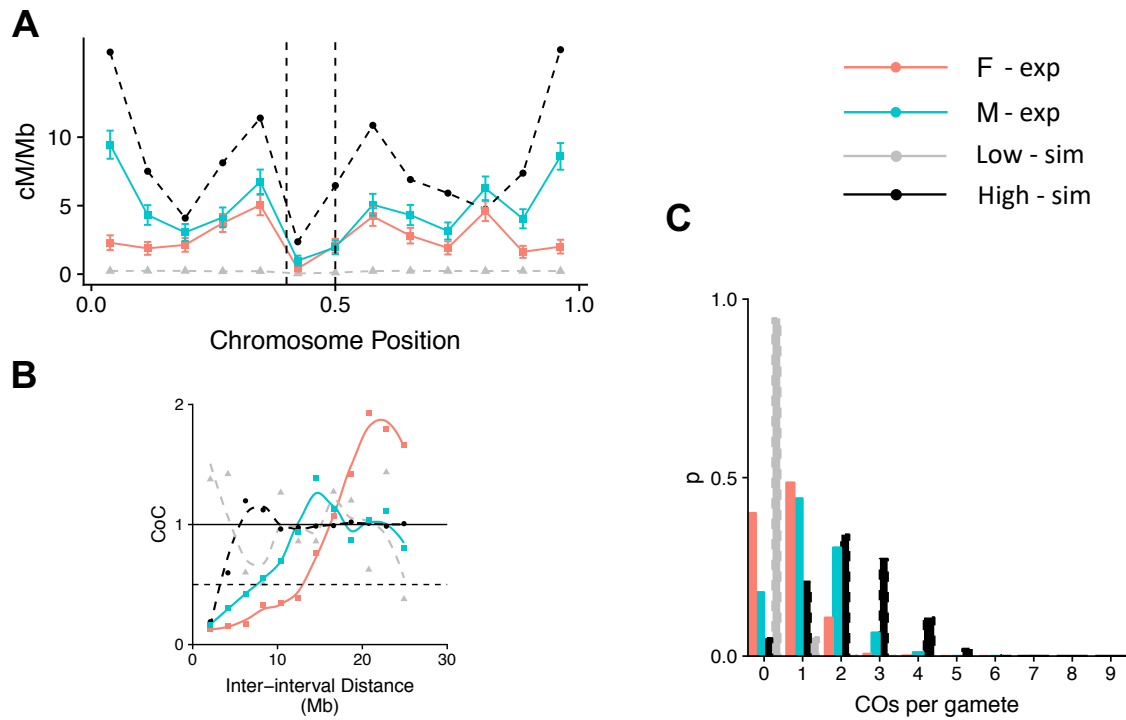
974



975

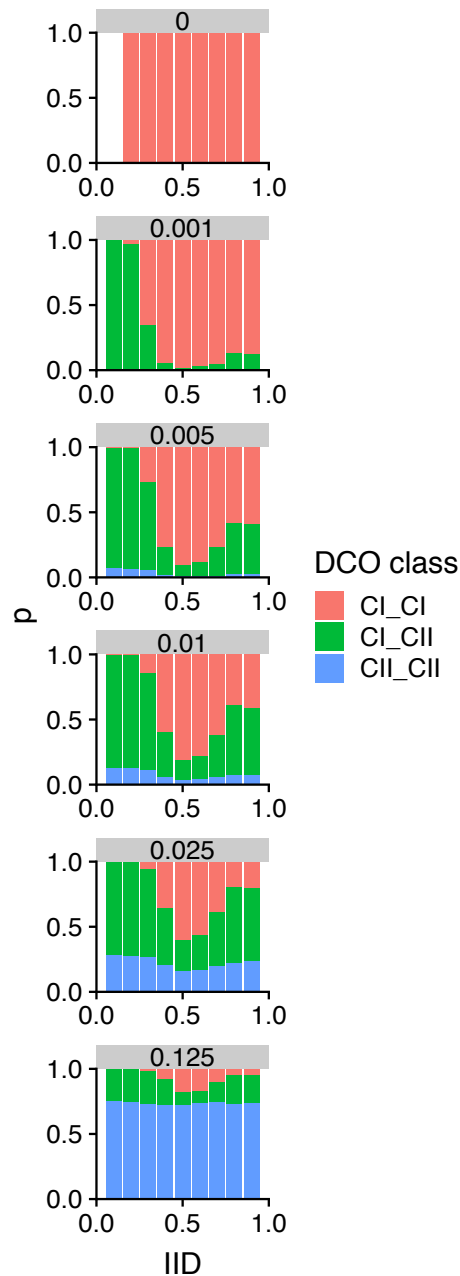
976

977 **Figure S2. CoC curves for simulated and experimental recombination data.** Each analysis
 978 includes experimental (solid lines) and simulated (dashed lines) data for male (blue) and female
 979 (orange). CoC curves with inter-interval distance measured in either Mb or $\mu\text{m SC}$ are shown. Male
 980 curves are shifted to the right relative to female curves when inter-interval distance is measured in
 981 Mb, but are similar when inter-interval distance is measured in $\mu\text{m SC}$. Male and female simulations
 982 shown assume 250 DSBs genome-wide. Chromosomes were divided into 13 equal-sized adjacent
 983 intervals for analysis



984
985

986 **Figure S3. Examples of simulated data that did not fit experimental data.** Each analysis shows
 987 experimental (solid lines) for male (blue) and female (orange) and simulated (dashed lines) data for
 988 high (black) and low (grey) recombining parameter sets. **A** Crossover distributions for Arabidopsis
 989 chromosome 5. Dashed lines represent the limits of the centromeric region over which precursor (DSB)
 990 number is markedly reduced both biologically (38) and during simulations. Error bars indicate 95%
 991 confidence intervals. **B** CoC curves for chromosome 5 with inter-interval distance (IID, the distance
 992 between a pair of genetic intervals) measured in Mb. **C** Event distribution for chromosome 5.
 993 Simulations shown assume 250 DSBs genome-wide. Chromosomes were divided into 13 equal-sized
 994 adjacent intervals for analysis.
 995



996

997 **Figure S4. Proportions of different double crossover (DCO) classes.** Charts show the proportions of

998 DCOs formed between two class I crossovers (CI_CI), two class II crossovers (CII_CII), or a class I and a

999 class II CO (CI_CII) for different IIDs and different values of T2Prob (grey bars). Total proportion of class

1000 II crossovers are as follows: T2Prob = 0, 0% class II COs; T2Prob = 0.001, 3% class II COs; T2Prob =

1001 0.005, 13% class II COs; T2Prob = 0.01, 23% class II COs; T2Prob = 0.025, 43% class II COs; T2Prob =

1002 0.125, 81% class II COs.